Drivers of Phytoplankton Bloom Interannual Variability in the Amundsen and Pine Island Polynyas

Guillaume Liniger[1,2*], Delphine Lannuzel[1,3,4], Sébastien Moreau[5,6], Michael S. Dinniman[7], Peter G. Strutton[1,3]

[1] Institute for Marine and Antarctic Studies, University of Tasmania, Hobart, Australia

[2] Monterey Bay Aquarium Research Institute, Moss Landing, CA, USA

[3] Australian Centre for Excellence in Antarctic Science, University of Tasmania, Hobart, Australia

[4] Australian Antarctic Program Partnership, University of Tasmania, Hobart, Australia

[5] Norwegian Polar Institute, Tromsø, Norway

[6] iC3: Centre for ice, Cryosphere, Carbon and Climate, Department of Geosciences, UiT The Arctic University of Norway, 9037 Tromsø, Norway

[7] Center for Coastal Physical Oceanography, Old Dominion University, Norfolk, VA, USA

* Corresponding Author: Guillaume Liniger (liniger@mbari.org)

Abstract

The Amundsen Sea Embayment (ASE) experiences both the highest ice shelf melt rates and the highest biological productivity in West Antarctica. Using 19 years of satellite data and modelling output, we investigate the long-term influence of environmental factors on the phytoplankton bloom in the Amundsen Sea (ASP) and Pine Island polynyas (PIP). We test the prevailing hypothesis that changes in ice shelf melt rate could drive interannual variability in the polynyas' surface chlorophyll-*a* (chl*a*) and Net Primary Productivity (NPP). We find that the interannual variability and long-term change in glacial meltwater may play an important role in chl*a* variance in the ASP, but not for NPP. Glacial meltwater does not explain the variability in both chl*a* and NPP in the PIP, where light and temperature are the main drivers. We attribute this to potentially greater amount of iron-enriched meltwater brought to the surface by the meltwater pump

downstream of the PIP, and the coastal ocean circulation accumulating and transporting iron towards the ASP.

Short Summary

We investigate the phytoplankton bloom variability and its drivers in the Amundsen polynyas (areas of open water within sea ice). Between 1998 and 2017, we find that changes in melting ice shelves may have different impacts on biological productivity between the Amundsen Sea (ASP) and Pine Island (PIP) polynyas. While ice shelves melting seems to play an important role for phytoplankton growth variability in the ASP, light and warmer waters appear to be more important in the PIP.

1. Introduction

Coastal polynyas are open ocean areas formed by strong katabatic winds pushing sea ice offshore (Morales Maqueda, 2004). They are the most biologically productive areas in the Southern Ocean (SO) relative to their size (Arrigo et al., 1998). This high biological productivity contrasts sharply with the rest of the SO, where low iron and light availability generally co-limit phytoplankton growth (Boyd et al., 2007). In West Antarctica, the Amundsen Sea Embayment (ASE) hosts two of the most productive Antarctic polynyas: The Pine Island Polynya (PIP) and Amundsen Sea Polynya (ASP) (Arrigo and van Dijken, 2003).

The phytoplankton community in the ASE is generally dominated by *Phaeocystis antarctica* (Lee et al., 2017; Yager et al., 2016), which is adapted to low iron availability and variable light conditions, and forms large summer blooms (Alderkamp et al., 2012; Yager et al., 2016). Diatoms like *Fragilariopsis sp*. and *Chaetoceros sp.* are also present, often becoming more important near the sea-ice edge or under shallow, stratified mixed layers where silicic acid (Si) and iron (Fe) are more available (Mills et al., 2012). In exceptional years, such as 2020, diatoms like *Dactyliosolen tenuijunctus* replaced *P. antarctica* as the dominant taxon, driven by anomalously shallow mixed layers and sufficient Fe–Si supply (Lee et al., 2022). This dynamic balance highlights how light, nutrient supply, and stratification control community composition in these highly productive and complex Antarctic systems.

The ASE is also the Antarctic region experiencing the highest mass loss from the Antarctic ice sheet. It has been undergoing increased calving, melting, thinning and retreat over the past three decades (Paolo et al., 2015; Rignot et al., 2013; Rignot et al., 2019; Shepherd et al., 2018). In the ASE, this ice loss is mainly through enhanced basal melting of the ice shelves. This is attributed to an increase in wind-driven Circumpolar Deep Water (CDW) fluxes and ocean heat content intruding onto the continental shelf through deep troughs such as the Pine Island and Dotson-Getz, and flowing into the ice shelves cavities (Dotto et al., 2019; Jacobs et al., 2011; Pritchard et al., 2012). There, warm waters fuel intense basal melt of the Pine Island, Thwaites, and Getz ice shelves, and returns as a fresher, colder outflow that can strengthen stratification (Jenkins et al., 2010; Ha et al., 2014). The PIP and ASP differ in their exposure to CDW and in local circulation: the ASP is more strongly influenced by upwelled modified CDW (mCDW) and glacial meltwater inputs, whereas in the PIP, vertical intrusions primarily occur beneath the ice shelves, leading to a more stratified and less directly ventilated surface layer (Assmann et al., 2013; Dutrieux et al., 2014). These hydrographic contrasts can shape the timing and magnitude of phytoplankton blooms and nutrient dynamics across the two polynyas.

Melting ice shelves can explain about 60% of the biomass variance between all Antarctic polynyas, suggesting that they are the primary supplier of dissolved iron (dFe) to coastal polynyas (Arrigo et al., 2015), and can directly or indirectly contribute to regional marine productivity (Bhatia et al., 2013; Gerringa et al., 2012; Hawkings et al., 2014; Herraiz-Borreguero et al., 2016). The strong melting of the ice shelves can release significant quantities of freshwater at depth (Biddle et al., 2017), resulting in a strong overturning within the ice shelves cavity, called the meltwater pump (St-Laurent et al., 2017). Modelling efforts have identified both resuspended Fe-enriched sediments and CDW entrained to the surface by the meltwater pump as the two primary sources of dFe to coastal polynyas, providing up to 31% of the total dFe, compared to 6% for direct ice shelves input (Dinniman et al., 2020; St-Laurent et al., 2017). Other drivers such as sea-ice coverage (and associated increases in light and dFe availability when sea ice retreats), or winds have also been shown to impact primary productivity in polynyas (Park et al., 2019; Park et al., 2017; Vaillancourt et al., 2003).

The key question of how glacial meltwater variability may impact biological productivity in the ASE has previously been raised during the ASPIRE program (Yager et al., 2012). During the expedition, a significant supply of melt-laden iron-enriched seawater to the central euphotic zone of the ASP was observed, potentially explaining why this area is the most biologically productive in Antarctica (Randall-Goodwin et al., 2015; Sherrell et al., 2015). Other studies in the Western Antarctic Peninsula and East Antarctica showed that the meltwater pump process was also responsible for natural Fe supply to the surface, increasing primary productivity (Cape et al., 2019; Tamura et al., 2022).

In this study, we investigate the long-term relationship between the main environmental factors of the ASE and the surface biological productivity, with a focus on ice shelves melting. A demonstrated relationship between glacial meltwater and phytoplankton growth would have far-reaching consequences for regional productivity in coastal Antarctica, and possibly offshore, over the coming decades under expected climate change scenarios (Meredith et al., 2019). We test the hypothesis that changes in glacial meltwater are linked to the surface ocean primary productivity variability observed over the last two decades. We use a combination of satellite (ocean color and ice shelf melting rate), climate re-analysis, and model data spanning 1998 to 2017.

2. Material and Methods

2.1 Study area and polynya mapping

We focus on the PIP and ASP in the ASE in West Antarctica (Fig. 1). The ASE is comprised of several ice shelves and glaciers, including: Abbot (Abb), Cosgrove (Cs), Pine Island (PIG), Thwaites (Tw), Crosson (Cs), Dotson (Dt) and Getz (Gt). The PIG and Thwaites have received significant attention in recent years due to their potentially large contribution to sea level rise (Rignot et al., 2019; Scambos et al., 2017). Along with the Crosson and Dotson ice shelves, the PIG and Thwaites are undergoing the highest melt rate, which is expected to increase under climate change scenarios (Naughten et al., 2023; Paolo et al., 2023). The mean mixed-layer depth (MLD) in the ASP is deeper (Fig. 1b), indicating that it may better entrain deeper sources

of nutrients into the upper waters. The polynyas' boundaries were determined using a 15% sea-ice concentration (SIC) mask (Moreau et al., 2015; Stammerjohn et al., 2008) for every 8-day period from June 1998 to June 2017 to accurately represent the size of the polynyas through time.

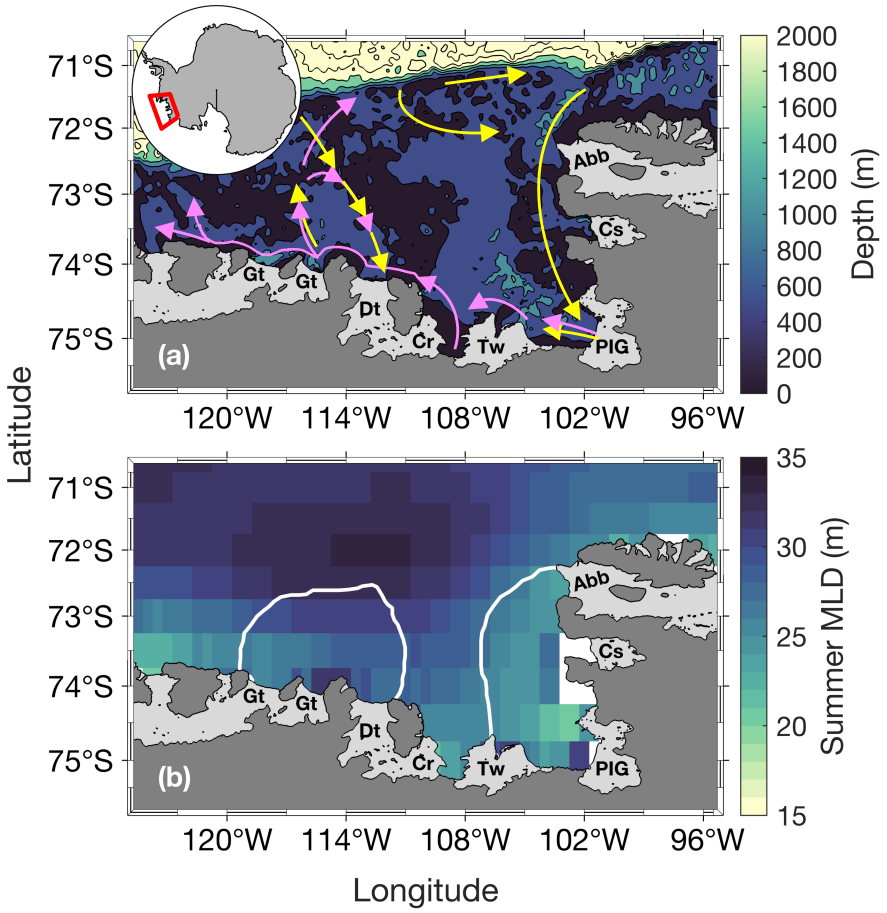

Figure 1. Study area. Panel 1a shows the bathymetry (from ETOPO1; Amante & Eakins, 2009) and panel 1b shows the climatological summer mixed-layer depth (MLD) from 1998 to 2017. Panel 1a shows a simplified schematic of the local deep ocean circulation (~ below 400m, yellow arrows) and upper glacial meltwater/sediments/circumpolar deep water sourced dFe pathways (magenta arrows), which follows the local upper ocean circulation. Schematic adapted from St-Laurent et al. (2017). The white lines in panel (b) represent the climatological summer polynyas' boundaries for the Amundsen Sea polynya (left) and Pine Island polynya (right). The dark grey area is mainland Antarctica. Light grey areas indicate floating ice shelves and glaciers: Abbot

(Abb), Cosgrove (Cs), Pine Island Glacier (PIG), Thwaites (Tw), Crosson (Cr), Dotson (Dt) and Getz (Gt).

2.2 Satellite ocean surface chlorophyll-*a* and net primary productivity

We obtained level-3 satellite surface chlorophyll-*a* (chl*a*) concentration with spatial and temporal resolution of 0.04° and 8 days from the European Space Agency (ESA) Globcolor project. We used the CHL1-GSM (Garver-Siegel-Maritorena) (Maritorena and Siegel, 2005) standard Case 1 water merged products consisting of the Sea-viewing Wide Field-of-view (SeaWiFS), Medium Resolution Imaging Spectrometer (MERIS), Moderate Resolution Imaging Spectroradiometer (MODIS-A) and Visible Infrared Imaging Suite sensors (VIIRS). We chose to perform our analysis with the merged GlobColour product, which has been widely applied and tested in Southern Ocean and coastal Antarctic studies (Ardyna et al., 2017; Sari El Dine et al., 2025; Golder & Antoine, 2025; Nunes, Fereira & Brito, 2025), to increase our spatial and temporal coverage.

We estimated phytoplankton bloom phenology metrics following the Kauko et al. (2021) method. Firstly, we applied a spatial 3x3 pixels median filter to reduce gaps in missing data. Then, if a pixel was still empty, we applied the average chl*a* of the previous and following week to fill the data gap. Data were smoothed using a 4-point moving median (representing a month of data). For each pixel, the threshold for the bloom detection was based on 1.05 times the annual median. The threshold method is frequently used (Racault et al., 2012; Siegel et al., 2002) and proven reliable at higher latitudes (Marchese et al., 2017; Soppa et al., 2016; Thomalla et al., 2023). We then determined 5 main bloom metrics. The bloom start (BS) is defined as the day where chl*a* first exceeds the threshold for at least 2 consecutive 8-day periods. Conversely, the bloom end is the day where chl*a* first falls below the threshold for at least 2 consecutive 8-day periods. The bloom duration (BD) is the time elapsed between bloom start and bloom end. The bloom mean chl*a* (BM) and bloom max chl*a* are respectively the average and maximum chl*a* value calculated during the bloom. Each year is centered around austral summer, from June 10th year *n* (day 1) to June 9th year *n+1* (day 365 or 366). We also averaged our 8-day data to monthly data to perform a spatial correlation analysis (see section 2.6).

We note that satellite ocean-colour chl*a* algorithms (including the GlobColour merged product used here) are globally tuned and may underperform in optically complex waters (e.g., with elevated dissolved organic matter or suspended sediments, 'Case 2'). In the ASP, past work (e.g., Park et al. 2017) shows that satellite chlorophyll climatologies reflect broad seasonal patterns that are consistent with *in situ* measurements of phytoplankton biomass and photophysiology, but there is limited data from regions immediately adjacent to glacier fronts or during times of strong meltwater input. Thus, while we consider satellite chl*a* to be useful for capturing spatial and temporal variability at polynya scale, uncertainty likely increases in optically complex zones near glacier margins or during low-light periods, and needs to be considered while interpreting results.

Eight-day satellite derived Net Primary Productivity (NPP) data with 1/12° spatial resolution, spanning 1998 - 2017 using the Vertically Generalized Production Model (Behrenfeld and Falkowski, 1997) were obtained from the Oregon State University website. The VGPM model is a chlorophyll-based approach and relies on the assumption that NPP is a function of chl*a*, influenced by light availability and maximum daily net primary production within the euphotic zone. SeaWiFS-based NPP data span 1998 - 2009, MODIS-based data span 2002 - 2017. To increase spatial and temporal coverage, we averaged SeaWiFS and MODIS from 2002 to 2009, where there was valid data for both in a pixel. NPP data were also monthly averaged and used to compare with chl*a* spatial and temporal patterns.

We caution that our study focuses on surface productivity, and satellites cannot detect under-ice phytoplankton and sea-ice algal blooms, therefore likely underestimating total primary productivity (Ardyna et al., 2020; Boles et al., 2020; Douglas et al., 2024; McClish & Bushinsly, 2023; Stoer & Fennel 2024).

2.3 Ice shelves volume flux

We used the latest ice shelf basal melt rate estimates from Paolo et al (2023). These estimates are derived from satellite radar altimetry measurements of ice shelves height, and produced on a 3

km grid every 3 months, with an effective resolution of ~5 km. For this study, our basal melt record spans June 1998 to June 2017. We calculated ice shelves volume flux rate for every gridded cell by multiplying the basal melt rate by the cell area. Data were summed for each ice shelf for a 3-month period. A 5-point (15 months) running mean was applied to reduce noise, such as spurious effects induced by seasonality on radar measurements over icy surfaces (Paolo et al., 2016), and data were temporally averaged from October to March to match the SO phytoplankton growth season (Arrigo et al., 2015), providing yearly mean values. The Abbot, Cosgrove, Thwaites, Pine Island Glacier, Crosson, Dotson and Getz ice shelves were used to calculate a single total meltwater volume flux (TVFall) for the ASE to investigate the link with surface chl*a* and NPP. We also investigated the relationship between each polynyas' productivity and their closest ice shelf. The Abbot, Cosgrove, PIG and Thwaites ice shelves were used to calculate the flux rate in the PIP (TVFpip) while the Thwaites, Crosson, Dotson and Getz ice shelves were chosen for the ASP (TVFasp). The Thwaites was used in both due to its central position between the two polynyas. We thereafter use the term glacial meltwater which defines meltwater resulting from ice shelf melting.

2.4 Simulated dFe distribution

The spatial distribution of dFe from different sources in the embayment was investigated from Dinniman et al. (2020) model output. The model used is a Regional Ocean Modelling System (ROMS) model, with a 5 km horizontal resolution and 32 terrain following vertical layers and includes sea-ice dynamics, as well as mechanical and thermodynamic interaction between ice shelves and the ocean. The model time run spans seven years and simulates fourteen different tracers to understand dFe supply across the entire Antarctic coastal zone, with the last two years simulating biological uptake. For the purpose of this study, we only use four different dFe sources/tracers in the ASE: ice shelf melt, CDW, sediments and sea ice. Each tracer estimation is independent from each other, meaning that one source does not affect the other, and they have the same probability for biological uptake by phytoplankton. That is, dFe from all sources can equally be taken up by phytoplankton. This is parametrized in the model as all iron molecules being bound to a ligand and therefore remaining in solution in a bioavailable form (Gledhill & Buck, 2012). For a detailed and complete explanation of the model, see Dinniman et al. (2020).

2.5 Other environmental parameters

We used SIC data spanning June 1998 to June 2017 from the National Snow and Ice Data Center (Cavalieri et al., 1996). The data are Nimbus-7 SMMR and SSMI/SSMIS passive microwave daily SIC with 25 km spatial resolution. We computed the sea-ice retreat time (IRT) and open water period (OWP) metrics using a 15% threshold (Stammerjohn et al., 2008). Daily data were monthly averaged to perform a spatial correlation analysis (see section 2.6).

We collected monthly level-4 Optimum Interpolation Sea Surface Temperature (OISST.v2) 0.25° high resolution dataset from the National Oceanic and Atmospheric Administration (Huang et al., 2021). Using this dataset compared to others has been proven to be the most suitable for our region of interest (Yu et al., 2023).

We obtained monthly Photosynthetically Available Radiation (PAR) from the same Globcolour project at the same spatial and temporal resolution (0.04° and 8 days) as chl*a*.

We used monthly averaged ERA5 reanalysis of zonal (u) and meridional (v) surface wind speed at 10 m above the surface (Hersbach et al., 2020).

We finally investigated monthly mean MLD from the Estimating the Circulation and Climate of the Ocean (ECCO) ocean and sea-ice state estimate project (ECCO consortium et al., 2021). The dataset is the version 4, release 4, at 0.5° spatial resolution.

2.6 Statistical analysis

Because some of our data were not normaly distributed, we consistently applied nonparametric tests throughout our statistical analysis. A Mann-Kendall test was performed to detect linear trends in chl*a* and NPP. A two-tailed non-parametric Spearman correlation metric (rho, p) was calculated to investigate the relationship between chl*a*, NPP, and glacial meltwater, as well as between phytoplankton and sea-ice phenology metrics. A two-tailed Mann-Whitney test was

277 performed to detect any significant mean differences for chl*a,* sea-ice phenology metrics, MLD,
278 PAR and dFe sources between the two polynyas. Monthly spatial correlations were tested
279 between SIC, winds, chl*a*, NPP, SST, and PAR after removing the seasonality for each
280 parameter. As well, a yearly spatial correlation between chl*a*, NPP and TVFall was performed.
281 The relationships between chl*a* concentration, NPP and environmental factors were explored
282 using a Principal Component Analysis (PCA). No pre-treatment (mean-centering or
283 normalization) was applied to the variables prior to PCA, as all variables are expressed in
284 comparable units and ranges, consistent with common practice in marine biogeochemistry
285 studies (Marchese et al., 2017; Liniger et al., 2020). Every statistical test was run with a 95% (p-
286 value < 0.05) confidence level. Our study spans 1998-2017. We are constrained by the start of
287 satellite ocean color data (1998) and the end of the ice shelf basal melt rate record (2017) from
288 Paolo et al (2023).
289
290 **3. Results**
291
292 3.1 Glacial meltwater and chl*a* variability
293
294 The annual climatology maps reveal substantially higher chl*a* concentration and NPP in the ASP
295 compared to the PIP (Fig. 2). The chl*a* concentration starts increasing in mid-November to reach
296 its average earlier in the PIP than the ASP. At its peak, chl*a* in the ASP is 6.49 mg m^{-3} and 4.94
297 mg m^{-3} in the PIP (Fig. 3a). During the bloom period, chl*a* concentration is also higher in the
298 ASP on average compared to the PIP (ASP = 5.21 ± 1.29 mg m^{-3} ; PIP = 3.69 ± 1.11 mg m^{-3},
299 Fig. 3b; Supplementary Table T1; p-value < 0.01). When looking at polynya area integrated
300 values (concentration multiplied by area gives units of mg m^{-1}), chl*a* is significantly higher in the
301 ASP than in the PIP, and increases with the polynya area (Supplementary Figs. S1 and S2). NPP
302 is also significantly higher in the ASP than in the PIP (1.88 ± 1.12 TgC y^{-1} vs 0.85 ± 0.86 TgC y^{-1}, p-value = 0.004; Supplementary Fig. S3). No significant interannual trends in mean chl*a* and
304 NPP during the bloom are observed for either polynya (Fig. 3b; Supplementary Fig. S3; p-
305 value > 0.1).
306

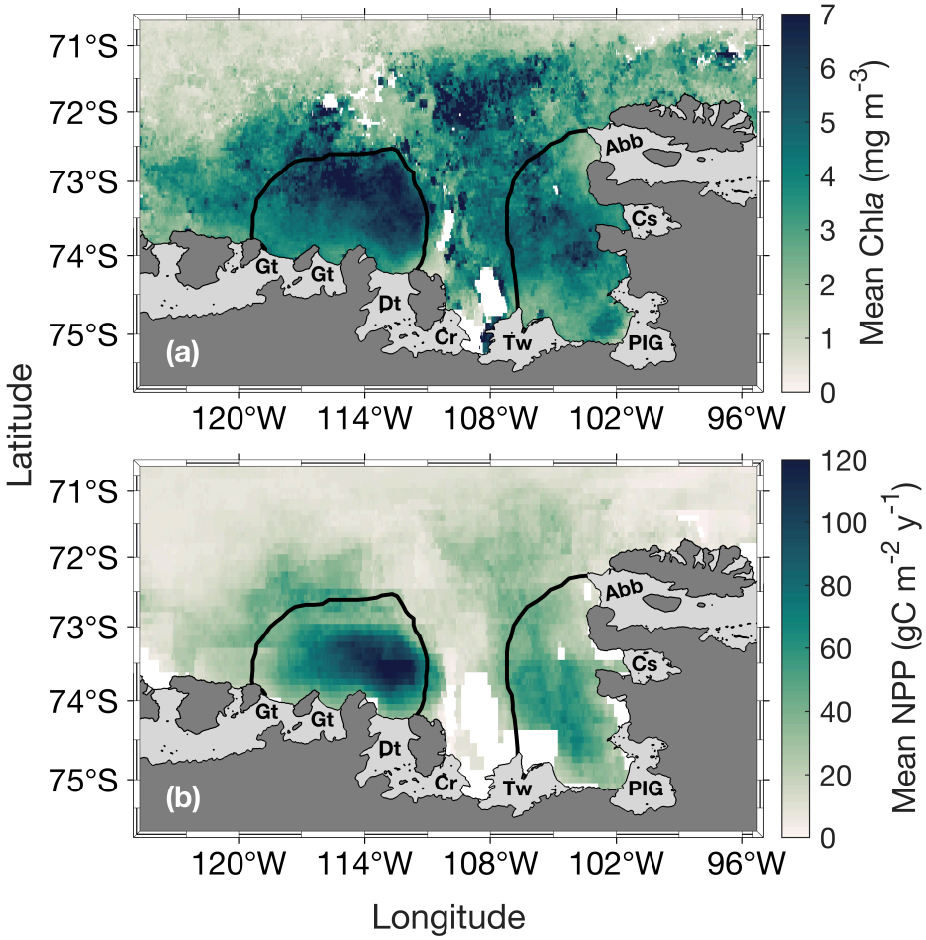

Fig. 2. Spatial distribution of (a) surface chlorophyll-*a* (chl*a*) during the bloom and (b) net primary productivity (NPP) climatology (1998 – 2017) for the Amundsen (ASP) and Pine Island (PIP) polynyas. The black lines represent the climatological summer polynyas' boundaries.

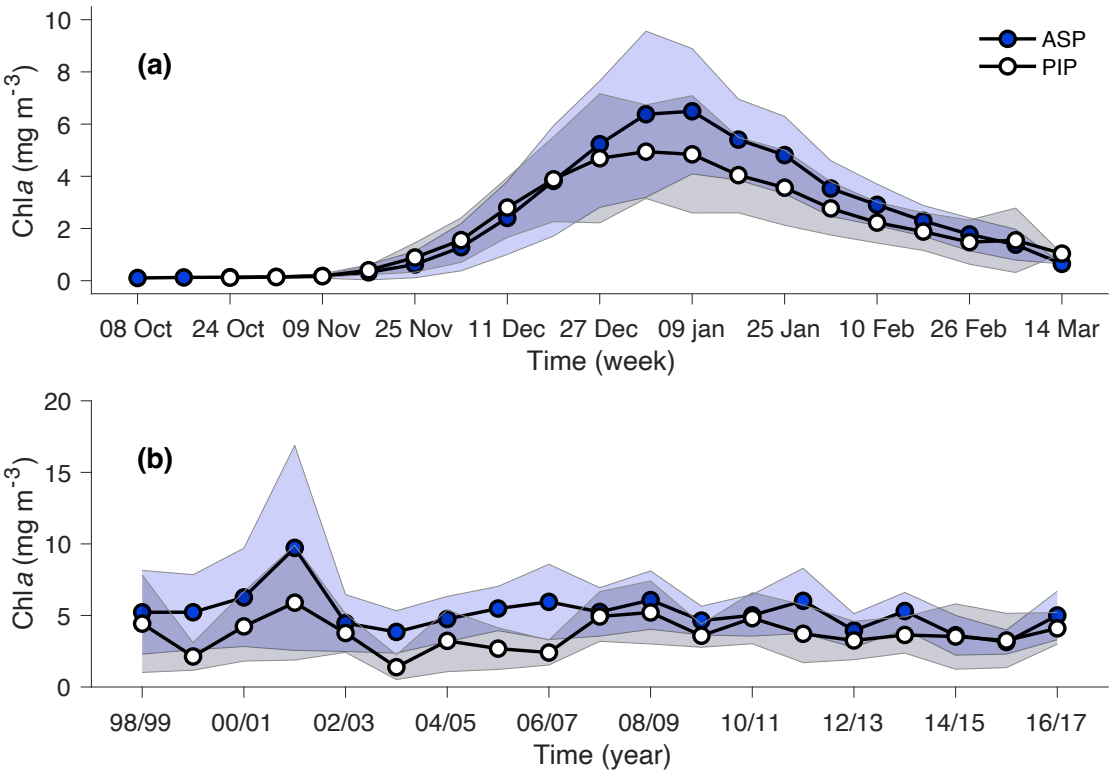

Fig. 3. (a) Weekly chlorophyll-*a* (chl*a*) climatology (1998-2017) for ASP (blue circles) and PIP (white circles). (b) Bloom mean chl*a* time series of ASP (blue circles) and PIP (white circles). Shadded areas respresent the standard devation for a given year. The relationship between chl*a* (in mg m^{-3} and mg m^{-1}) and the polynya size is shown in Supplementary Fig. S2.

The variability in TVFall is statistically uncorrelated with surface ch*la* concentration and NPP in both polynyas from 1998 to 2017 (Fig. 4; Supplementary Fig. S4). However, the relationship becomes strongly significant in the ASP for both mean and max chl*a* when we remove the chl*a* outlier in 2001/02 (red data point; Figs. 4a-b), although not for NPP (Supplementary Figs. S4a-b). The positive relationship implies that surface chl*a* in the ASP is higher when more glacial meltwater is delivered to the embayment. No strong relationships are observed in the PIP between TVFall, surface chl*a* and NPP (Figs. 4c-d; Supplementary Figs. S4c-d). When fluxes from individual glaciers are considered, PIP chl*a* does not correlate with Abbot, Cosgrove, PIG, Thwaites or TVFpip fluxes (Table 1). On the other hand, ASP chl*a* shows strong relationships with TVFasp, the Dotson and Crosson ice shelves (Table 1), and all ice shelves become

significantly correlated with mean and max chl*a* when year 2001/02 is removed. There are no statistically significant relationships between individual ice shelves and NPP in both polynyas. Spatially, the mean and max chl*a* are strongly correlated with TVFall in southern-eastern part of the ASP, in front of the Dotson ice shelf (Figs. 5a-b), where a positive relationship with NPP is also observed (Fig. 5c), although not significant.

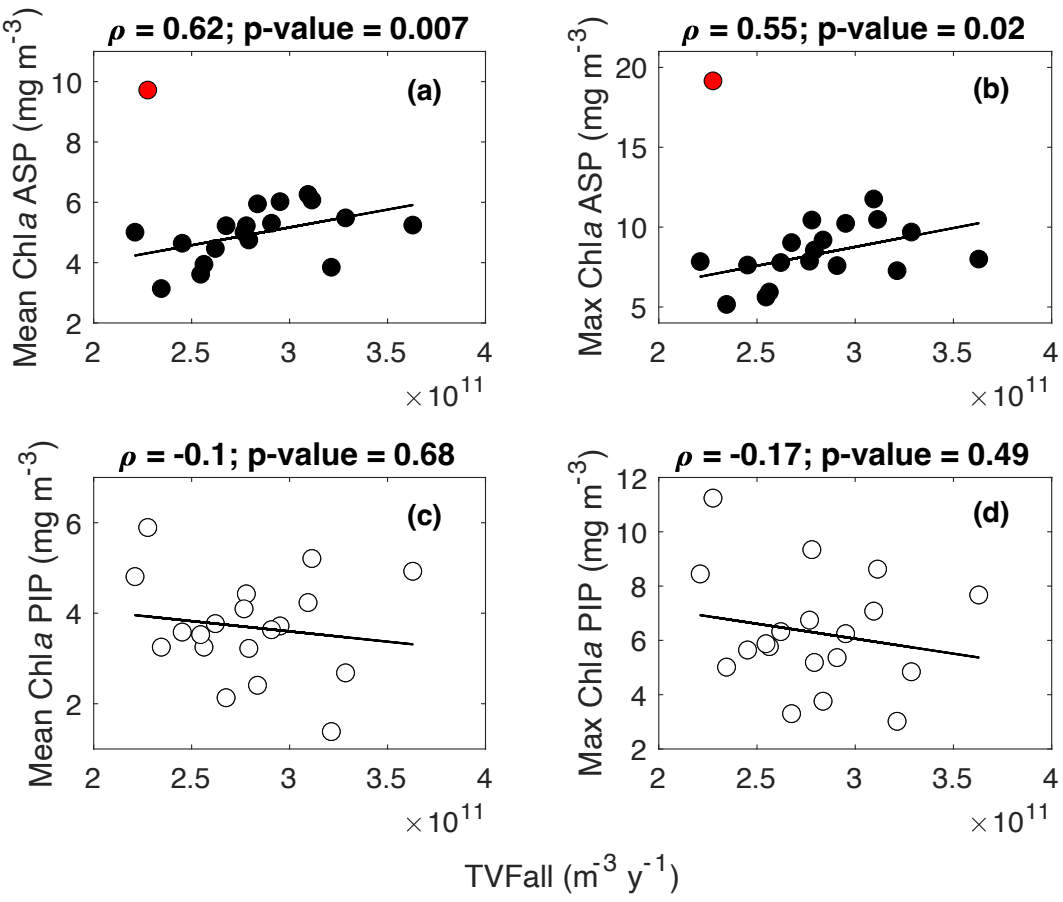

Fig. 4. Scatter plots of mean and max surface chlorophyll-*a* (chl*a*) with the total volume flux (TVFall) for (a-b) the ASP and (c-d) the PIP from 1998 to 2017 (n=19). The fitted lines and statistics exclude year 2001/02 (red outlier) for the ASP regressions. If all data is considered, the relationships between mean chl*a*, max chl*a* and TVFall in the ASP are not significant. TVFall is an annual integral representing the sum of all ice shelves (see methods section) for the ASE.

Table 1. Statistical summary of the relationships between ice shelves volume flux and

surface chlorophyll-*a* (chl*a*). The * marks a significant (p-value < 0.05) relationship. Statistical results for the ASP include all years (n=19). All relationships between mean chl*a*, max chl*a* and ASP ice shelves become significant when year 2001/02 is removed.

	ASP				PIP			
	Mean chl*a*		Max chl*a*		Mean chl*a*		Max chl*a*	
	rho	p-value	rho	p-value	rho	p-value	rho	p-value
Abbot	/	/	/	/	0.09	0.73	-0.04	0.88
Cosgrove	/	/	/	/	-0.32	0.18	-0.46	0.05
PIG	/	/	/	/	-0.04	0.88	-0.13	0.61
Thwaites	0.16	0.52	0.11	0.66	0.12	0.63	0.09	0.71
Crosson	0.43	0.07	**0.50**	**0.03***	/	/	/	/
Dotson	**0.48**	**0.04***	**0.54**	**0.02***	/	/	/	/
Getz	0.37	0.12	0.43	0.07	/	/	/	/
TVFasp	0.42	0.07	**0.46**	**0.05***	/	/	/	/
TVFpip	/	/	/	/	0.009	0.97	-0.1	0.68

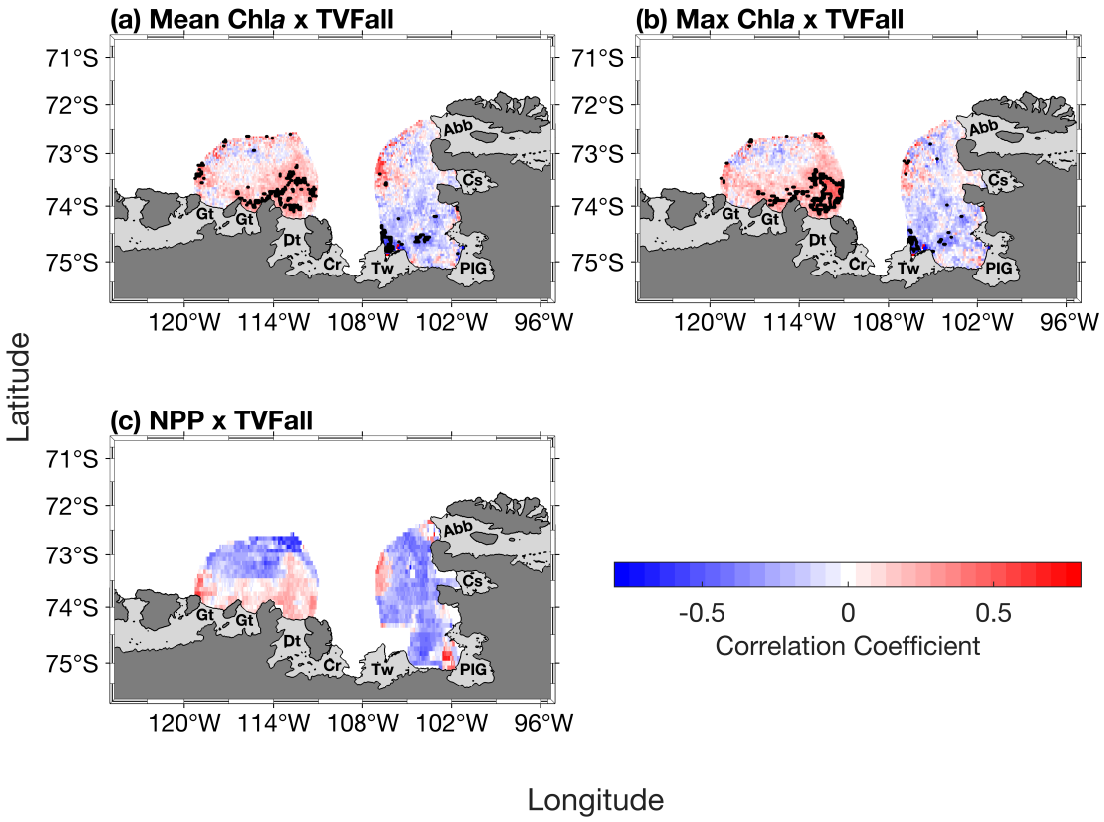

Fig. 5. Spatial correlation maps between total volume flux (TVFall) and (a) surface mean chlorophyll-*a* (chl*a*), (b) surface max chl*a* and (c) net primary productivity (NPP) (n=19). The black contour represents significant correlations at 95% confidence level. Data outside of the summer climatological polynyas' boundaries were masked out.

3.2 Simulated dFe sources distribution

The modelled spatial distribution of surface dFe sources is presented in Fig. 6. On average, the smallest dFe source in the embayment is from the ice shelves, with a maximum concentration between the Thwaites and Dotson ice shelves. The dFe from sea ice is slightly higher than from ice shelves and similar over the two polynyas, and is higher near the sea-ice margin (Fig. 6b). The dFe from CDW is also higher between the Thwaites and Dotson (Fig. 6c). Sediment is the dominant dFe source (Fig. 6d). Its distribution spreads from 108°W to the western part of the Getz ice shelf. The highest sediment concentration is found along the coast and inside the ASP. On

polynya-wide average basis, the sediment reservoir contributes significantly more to total dFe in the ASP (58.3%, 0.13nM) compared to sea ice (16.5%, 0.04nM), CDW (13.5%, 0.03nM) and ice shelves (11.7%, 0.03nM). In the PIP, the contribution of sediments is still significantly higher (41.2%; 0.08nM) but lower than the ASP and the contribution gap with the other sources decreases. The CDW and sea ice contribute 22.5% (0.04nM) and 18.9% (0.035nM) to the dFe pool respectively, while ice shelves are still the smallest sources at 14.5% (0.03nM) in the PIP.

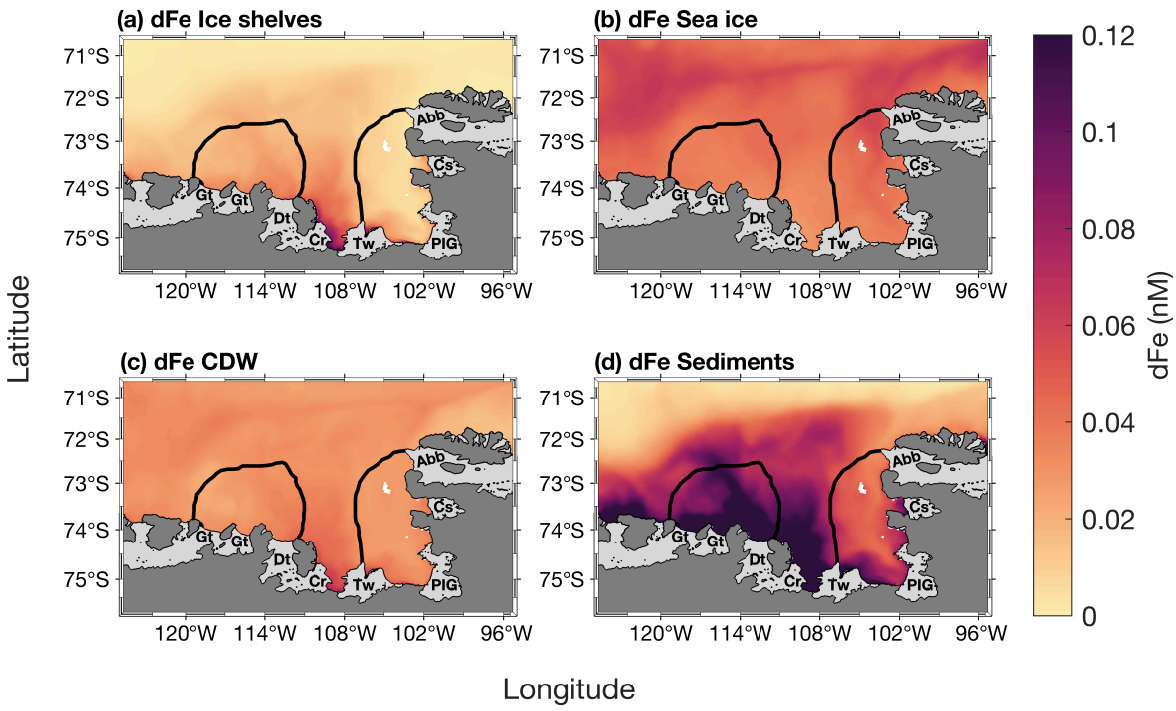

Fig. 6. Two-years top-100m averaged spatial distribution of surface dissolved iron (dFe) contribution from (a) ice shelves, (b) sea ice, (c) circumpolar deep water (CDW) and (d) sediments simulated by the model from Dinniman et al. (2020). The black lines represent the climatological summer polynyas' boundaries.

3.3 Environmental parameters, chl*a* and NPP variability

During the phytoplankton growth season (October-March), SIC is spatially significantly anticorrelated to the meridional winds speed in both polynyas (Fig. 7a). Chl*a* is significantly positively correlated with SST in the eastern ASP, and the whole PIP (Fig. 7b), but weakly with

PAR in both polynyas (Fig. 7c). Finally, PAR and SST are positively related in both central polynyas, albeit not significantly (Fig. 7d). We note that similar spatial relationships are observed when NPP is correlated with SST and PAR. (Supplementary Fig. S5).

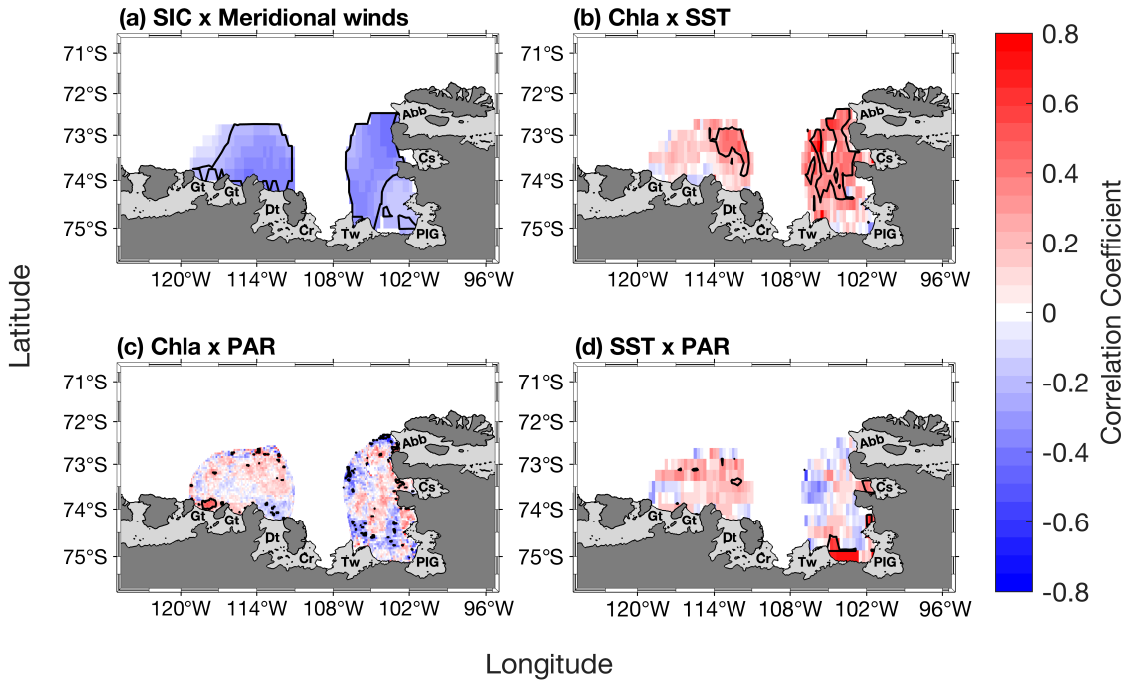

Fig. 7. Spatial correlation map between sea-ice concentration (SIC) and (a) meridional winds. Spatial correlation maps between mean chlorophyll-*a* (chl*a*) concentration and (b) sea surface temperature (SST), (c) photosynthetically available radiation (PAR). (d) Spatial correlation map between PAR and SST. Data span 1998 – 2017 from October to March (n=114). The black contour represents significant correlations at 95% confidence level. Seasonality was removed from the data before performing the correlation. Data outside of the summer climatological polynyas' boundaries were masked out.

Regarding the phenology, the bloom start is positively correlated to IRT and negatively with OWP in the ASP, although not significantly with the OWP (Table 2). This means that the bloom starts earlier and later as IRT does, and that longer OWP and earlier bloom starts are correlated with earlier ice retreat. The bloom mean and bloom max chl*a* are not correlated with either IRT and OWP in the ASP. IRT and OWP are significantly related (p = -0.93; p-value < 0.001). When

year 2001/02 is removed, no significant changes in the relationships between all parameters are detected. In the PIP, all metrics are significantly related to each other, except for PAR and OWP (Table 2). That is, the bloom start is positively correlated with IRT and negatively with OWP, while the bloom duration, mean chl*a*, max chl*a* concentrations and NPP are negatively linked to the IRT and positively with OWP. SST and PAR are negatively correlated with IRT, and positively with SST. IRT and OWP are significantly related in the PIP (p = -0.88; p-value < 0.001).

Table 2. Statistical summary of the relationships between the phytoplankton bloom metrics and environmental parameters (n=19). The * marks a significant (p-value < 0.05) relationship. IRT = ice retreat time, OWP = open water period, NPP = net primary productivity, SST = sea surface temperature, PAR = photosynthetically available radiation. Removing year 2001/02 for the ASP slightly changes the strength of the relationships between parameters (i.e., rho) but not the significance.

	Amundsen Sea polynya				Pine Island polynya			
	IRT		OWP		IRT		OWP	
	rho	p-value	rho	p-value	rho	p-value	rho	p-value
Bloom start	**0.51**	**0.03***	-0.43	0.07	**0.56**	**0.02***	**-0.48**	**0.04***
Bloom duration	-0.12	0.63	0.09	0.71	**-0.56**	**0.02***	**0.59**	**0.01***
Bloom mean	0.19	0.44	-0.33	0.17	**-0.67**	**0.003***	**0.50**	**0.04***
Bloom max	0.24	0.32	-0.35	0.14	**-0.65**	**0.005***	**0.52**	**0.03***
NPP	**-0.55**	**0.02***	0.45	0.05	**-0.72**	**0.001***	**0.54**	**0.02***
SST	-0.09	0.72	-0.01	0.96	**-0.57**	**0.02***	**0.52**	**0.03***
PAR	-0.09	0.72	0.05	0.84	**-0.62**	**0.007***	0.38	0.12

We explore the relationships between phytoplankton bloom phenology metrics and their potential environmental drivers by conducting a multivariate PCA for both polynyas (Fig. 8). The PCA reduces our datasets (11 variables) and breaks them down into dimensions that capture most of the variability and relationships between all variables. Arrows indicate the contribution of each variable to the dimensions, with longer arrows representing stronger influence. Observations (in our case, years) positioned in the direction of an arrow are more influenced by that variable. In the ASP (Fig. 8a), the first two principal components explain 55.3% of the total variance (Dim1: 35%, Dim2: 20.3%). NPP in the ASP is closely associated with BD, indicating that the bloom duration is the primary driver of production. On the other hand, environmental vectors such as TVFall and TVFasp project more strongly onto Dim2 with the bloom mean chl*a*, indicating that meltwater input may influence surface chl*a* interannual variability, and is less directly tied to NPP. We note that when year 2001/02 is removed, the relationship between TVFasp and TVFall becomes much stronger with the bloom mean chl*a* (Supplementary Fig. S6a) and is slightly anticorrelated to SST and MLD. In the PIP (Fig. 8b), the first two components account for 63.7% of the total variance (Dim1: 46.7%, Dim2: 17%). Compared to the ASP, both NPP and BM cluster strongly with BD and PAR on Dim1. Additionally, IRT, OWP and SST and MLD aligned along Dim1, which explains 46.7% of the total variance compared to 35% for the ASP, suggesting that physical conditions might play a stronger structuring role in PIP compared to the ASP. In contrast, TVFall and TVFpip stand alone and align more strongly with Dim2, suggesting a less dominant influence of meltwater on the system bloom mean chl*a* and NPP variability in the PIP. Finally, polynya-averaged PAR and MLD are significantly stronger and deeper, respectively, in the ASP compared to the PIP during the bloom season (MLD ASP = 28.5 ± 5.7m; MLD PIP = 24.9 ± 3.7m; p-value = 0.03 and PAR ASP = 31.5 ± 5.4 Einstein m^{-2} d^{-1} ; PAR PIP = 26.5 ± 6.7 Einstein m^{-2} d^{-1}; p-value = 0.02).

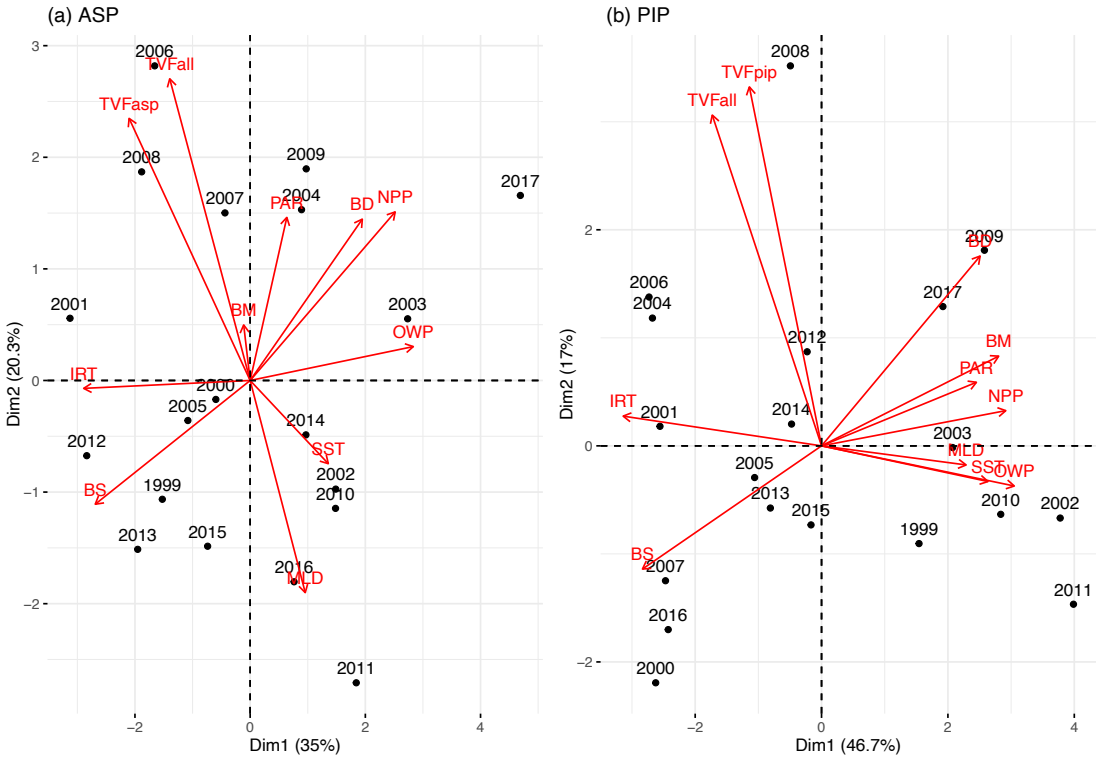

Fig. 8. Principal component analysis biplot of environmental parameters (red) and years (black) for (a) the ASP and (b) the PIP. TVFasp = total volume flux for ASP; TVFpip = total volume flux for PIP; TVFall = total volume flux for all ice shelves; BM = bloom mean; PAR = photosynthetically available radiation; BD = bloom duration; NPP = net primary productivity; OWP = open water period; SST = sea surface temperature; MLD = mixed-layer depth; BS = bloom start; IRT = ice retreat time. The same plot is presented in supplementary Fig. S6, but removing year 2001/02 for the ASP, emphasizing the relationship between total volume flux (TVFall, TVFasp) and BM in the ASP.

4. Discussion

4.1 Effect of glacial meltwater on phytoplankton chl*a* and NPP

The relationship between glacial meltwater, surface chl*a* and NPP observed over the last two decades was distinctly different between the two polynyas. In the ASP, we found that enhanced

605 glacial melt translates into higher surface chl*a*, but not with NPP (when removing year 2001/02;
606 Figs. 4a-b; Supplementary Fig. S6a). Modelling results (Fig. 6) suggest that sediment from the
607 seafloor is the main source of dFe in the ASP, but this source is also linked to glacial melt. Ice
608 shelf glacial meltwater drives the meltwater pump, which brings up mCDW and fine-grained
609 subglacial sediments to the surface. This result is in agreement with previous research: Melt-
610 laden modified CDW flowing offshore from the Dotson ice shelf to the central ASP (Sherrell et
611 al., 2015), and resuspended sediments (Dinniman et al., 2020; St-Laurent et al., 2017; 2019) have
612 been identified as significant sources of dFe to be used by phytoplankton. Interestingly, both dFe
613 supplied from ice shelves and CDW are most important in front of the Thwaites and Crosson ice
614 shelves, where the area averaged basal melt rate, and thus likely the area averaged meltwater
615 pumping (Jourdain et al., 2017), are typically strongest in observations (Adusumilli et al., 2020;
616 Rignot et al., 2013) and the modelling (Fig. 6). The year 2001/02 does not stand out as being
617 influenced by any specific parameter in the ASP compared to other years (Fig. 8a,
618 Supplementary Fig. S6a). The anomalously high surface chl*a* observed during this year, as also
619 reported by Arrigo et al. (2012), may result from exceptional conditions that were not captured
620 by the parameters analysed in our study, for instance, an imbalance in the grazing pressure.
621 Interestingly, surface chl*a* and NPP exhibit contrasting trends when averaged across the polynya.
622 While TVFall may explain some of the variance in surface chl*a*, it does not account for the
623 variance in NPP, whether assessed through direct or multivariate relationships. This decoupling
624 between chl*a* and NPP in the ASP suggests that glacial meltwater, while enhancing surface
625 phytoplankton biomass through nutrient delivery, may also promote vertical mixing. This mixing
626 deepens the mixed layer, reducing light availability and constraining photosynthetic rates. These
627 rates are influenced by fluctuations in the MLD, even in the presence of high biomass and
628 sufficient macronutrients. The summer MLD is deeper in the ASP (Fig. 1b), which would
629 decrease light availability, despite higher PAR compared to the PIP. Previous studies report that
630 the small prymnesiophyte *P. antarctica,* a low-efficiency primary producer (Lee et al., 2017), is
631 better adapted to deeper mixed layers and therefore lower light conditions (Alderkamp et al.,
632 2012; Mills et al., 2010) and could contribute to high surface chl*a* decoupled from NPP, as
633 observed in the ASP. This is consistent with past *in situ* studies showing systematic differences
634 in mixed-layer structure between the two polynyas. The PIP commonly exhibits a shallow,
635 strongly stratified surface mixed layer while the ASP is more variable and has been observed to

host deeper MLD (Alderkamp et al., 2012; Park et al., 2017; Yager et al., 2016; Mills et al., 2012).

In the PIP, we did not find any long-term relationships between the phytoplankton bloom, NPP and glacial meltwater. Variability in ice shelf glacial meltwater may not have the same effect on the surface chl*a* and NPP in the PIP compared to the ASP. Iron delivered from glacial melt process related in the PIP and west of it could accumulate and follow the westward coastal current, towards the ASP (St-Laurent et al., 2017). These sources would include dFe from meltwater pumped CDW, sediments and ice shelves, all of which are higher in front of the Crosson ice shelf, west of the PIP (Fig. 6). With the coastal circulation, this would make dFe supplied by glacial meltwater greater in the ASP, thereby contributing to the higher productivity in the ASP. Recently, subglacial discharge (SGD) was shown to have a different impact on basal melt rate in the ASE polynyas (Goldberg et al., 2023), where PIG had a lot less relative increase in melt with SGD input than Thwaites or Dotson/Crosson. Thus, assuming a direct relationship between meltrate, SGD and dFe sources, the signal in the PIP (fed by PIG melt) will be much weaker than in the ASP (fed by upstream Thwaites, Crosson and local Dotson due to the circulation), which might also explain the discrepancies between the PIP and ASP. A stronger meltwater-driven stratification may also dominate in the PIP, reducing vertical nutrient replenishment and thereby limiting biomass growth (Oh et al., 2022), even where TVFall is high, hence leading to a direct negative relationship observed compared to the ASP (Fig. 4; Supplementary Fig. S4). The model outputs used here are critical to understand the spatial distribution of dFe in the embayment. They strongly suggest, but do not definitively demonstrate, the role of dFe in influencing the phytoplankton bloom interannual variability.

The decoupling between surface chl*a* and NPP could reflect two contrasting meltwater effects. Near glacier and ice-shelf fronts, entrainment of iron-rich deep waters rising to the surface through the meltwater pump can produce surface chl*a* maxima (high biomass) without proportional increases in depth-integrated productivity. Further from the coast, meltwater spreading at neutral buoyancy strengthens stratification, limiting vertical nutrient fluxes and thereby suppressing NPP despite elevated chl*a*. These dual mechanisms are consistent with observational and modelling studies of meltwater entrainment and dispersal (Randall-Goodwin et

al., 2015; St-Laurent et al., 2017; Dinniman et al., 2020; Forsch et al. 2021), and suggest that spatial heterogeneity in plume dynamics could explain the observed chl*a* and NPP mismatch. We also note as a limitation that satellite-derived chl*a* and VGPM NPP estimates lack the vertical resolution needed to resolve sub-plume stratification and mixing processes (e.g., fine-scale vertical gradients in iron or nutrient fluxes), so our mechanistic interpretations of surface chl*a* vs. depth-integrated productivity decoupling must be taken with caution.

Satellite algorithms commonly estimate NPP from surface chl*a*, but the approach and assumptions vary across models. The VGPM relates chl*a* to depth-integrated photosynthesis through empirical relationships with light and temperature (Behrenfeld & Falkowski, 1997). In contrast, the Carbon-based Productivity Model (CbPM) emphasizes phytoplankton carbon biomass and growth rates derived from satellite optical properties, decoupling productivity estimates from chl*a* alone (Westberry et al., 2008). The CAFE model (Carbon, Absorption, and Fluorescence Euphotic-resolving model) integrates additional physiological parameters such as chl*a* fluorescence and absorption to better constrain phytoplankton carbon fixation (Silsbe et al., 2016). In the Southern Ocean, where light limitation, iron supply, and community composition strongly influence the relationship between chl*a* and productivity, these algorithmic differences can yield substantial variability in NPP estimates (Ryan-Keogh et al., 2023), with studies showing that VGPM-type models often outperform CbPM in coastal Southern Ocean regions (Jena et al., 2020). Because the VGPM algorithm does not explicitly incorporate the MLD, but instead estimates primary production integrated over the euphotic zone based on surface chl*a*, PAR, and temperature, it may not fully capture the influence of variable MLD or subsurface processes related to glacial melt, which could contribute to the observed decoupling between chl*a* and NPP. Therefore, while the observed decoupling between chl*a* and NPP in the ASP might also come from our choice of dataset, the VGPM model may be more appropriate for coastal polynya environments, such as those in the Amundsen Sea.

Direct observations from Sherrell et al. (2015) showed higher chl*a* in the central ASP while surface dFe was low weeks before the bloom peak. This suggests a continuous supply and consumption of dFe in the area, most likely from the cicrculation, as mentioned above. Considering the long residence time of water masses in both polynyas (about 2 years (Tamsitt et

al., 2021)), and the daily dFe uptake by phytoplankton (3-196 pmol l^{-1} d^{-1} (Lannuzel et al., 2023)), we also hypothesise that any dFe reaching the upper ocean from external sources is quickly used and unlikely to remain readily available for phytoplankton in the following spring season.

In recent model simulations with the meltwater pump turned off, Fe becomes the principal factor limiting phytoplankton growth in the ASP (Oliver et al., 2019). However, the transport of Fe-rich glacial meltwater outside the ice shelf cavities and to the ocean surface depends strongly on the local hydrography. While Naveira Garabato et al. (2017) suggested that the glacial meltwater concentration and settling depth (neutral buoyancy) outside the ice shelf cavities is controlled by an overturning circulation driven by instability, others suggest that the strong stratification plays an important role in how close to the surface the buoyant plume of said meltwater can rise (Arnscheidt et al., 2021; Zheng et al., 2021). Therefore, high melting years and greater TVFall might not necessarily translate into a more iron-enriched meltwater delivered to the surface outside the ice shelf cavities, close to the ice shelf edge, as rising water masses may be either prevented from doing so, or be transported further offshore in the polynyas where the phytoplankton bloom occurs, before they can resurface (Herraiz-Borreguero et al., 2016).

Although several Fe sources can fuel polynya blooms, and they depend on processes mentioned above, Fe-binding ligands may ultimately set the limit on how much of this dFe stays dissolved in the surface waters (Gledhill and Buck, 2012; Hassler et al., 2019; Tagliabue et al., 2019). Models of the Amundsen Sea (Dinniman et al., 2020, 2023; St-Laurent et al., 2017, 2019) did not include Fe complexation with ligands and assumed a continuous supply of available dFe for phytoplankton. Spatial and seasonal data on Fe-binding ligands along the Antarctic coast remain extremely scarce and their dynamics are poorly understood (see Smith et al. (2022) for a database of publicly available Fe-binding ligand surveys performed south of 50°S). Field observations in the ASP and PIP suggest that the ligands measured in the upwelling region in front of the ice shelves had little capacity to complex any additional Fe supplied from glacial melt. As a consequence, much of the glacial and sedimentary Fe supply in front of the ice shelves could be lost via particle scavenging and precipitation (Thuróczy et al., 2012). This was also recently observed by van Manen et al. (2022) in the ASP. However, within the polynya

blooms, Thuróczy et al. (2012) found that the ligands produced by biological activity were capable of stabilising additional Fe supplied from glacial melt, where we observed the highest productivity. The production of ligands by phytoplankton would increase the stock of bioavailable dFe and further fuel the phytoplankton bloom in the polynyas, potentially highlighting the dominance of *P. antarctica*, which uses iron-binding ligands more efficiently than diatoms (Thuróczy et al., 2012), even under low light conditions. Model development and sustained field observations on dFe availability, including ligands, are needed to adequately predict how these may impact biological productivity under changing glacial and oceanic conditions, now and in the future.

Overall, the discrepancies observed between the ASP and PIP point to a complex set of ice-ocean-sediment interactions, where several co-occurring processes and differences in hydrographic properties of the water column influence dFe supply and consequent primary productivity.

4.2 Possible drivers of the difference in phytoplankton surface chl*a* and NPP between the two polynyas

The biological productivity is higher in the ASP than the PIP, consistent with previous studies (Arrigo et al., 2012; Park et al., 2017). In section 4.1, we mentioned the underlying hydrographic drivers of these differences. We related the higher biological productivity in the ASP to a potentially greater supply of iron from melt-laden Fe-enriched mCDW and sediment sources, but this difference in productivity could also be attributed to other local features. The Bear Ridge grounded icebergs on the ASP's eastern side (Bett et al., 2020) could add to the overall meltwater pump strength. They can enhance warm CDW intrusions to the ice shelf cavity (Bett et al., 2020), increasing ice shelf melting and subsequent stronger phytoplankton bloom from the meltwater pump activity. These processes are weaker or absent in the PIP. Few sources other than glacial meltwater may influence the bloom in the PIP. For instance, dFe in the euphotic zone can also be sustained by the biological recycling, as shown in the PIP by Gerringa et al. (2020).

760 Sea ice could also partly explain the difference in chl*a* magnitudes, NPP, and variability between
761 the ASP and PIP. The strong spatial correlation between SIC and meridional winds (Fig. 7a)
762 indicates that southerly winds can export the coastal sea ice offshore and play a significant role
763 in opening the polynyas. In the ASP compared to the PIP, sea ice retreats earlier (IRT = Jan 1st ±
764 14d vs Jan 18th ± 17d, p-value = 0.003), the open water period is longer (OWP = 61 ± 16d vs 44
765 ± 22d, p-value < 0.001), and the SIC is lower (Supplementary Fig. S7). In the ASP, an early sea-
766 ice retreat leads to an earlier bloom start, but the longer open water period is not significantly
767 associated with greater bloom mean and max chl*a* (Table 2). On the other hand in the PIP, an
768 early sea-ice retreat also triggers an early bloom start, but the longer open duration is associated
769 with warmer water, higher bloom mean chl*a*, max chl*a*, and NPP. These results suggest that
770 different processes might drive phytoplankton growth variability in the two polynyas. In the
771 ASP, it is likely the replenishment of dFe mentioned above that mostly influences the bloom. In
772 the PIP, higher SIC can delay the retreat time and shorten the open water season (Table 2,
773 Supplementary Fig. S7), leading to lower chl*a* and NPP compared to the ASP. The significant
774 negative relationships between IRT, PAR, chl*a* and NPP in the PIP (Table 2, Supplementary Fig.
775 S6) suggests a strong light limitation relief in the polynya. This light limitation hypothesis is
776 further supported by the high correlation between polynya-averaged chl*a* mean with PAR and
777 SST in the PIP across the 19 years of study, compared to the lack of correlation in the ASP
778 (Supplementary Table T2; p-value < 0.01 for all relationships in the PIP). While *P. antarctica* is
779 usually the main phytoplankton species dominating in both polynyas, the combination of light-
780 limitation relief and higher SST may create better conditions for a stratified and warmer
781 environment that would favor diatom (Arrigo et al., 1999; van Leeuwe et al., 2020), as recently
782 observed in the ASP (Lee et al., 2022). The positive association of PAR, SST and chl*a* with
783 MLD likely reflects conditions around sea-ice retreat (all negatively associated with IRT), when
784 enhanced wind mixing deepens the mixed layer and replenishes surface nutrients while light
785 availability and SST increases. This nutrient-light co-limitation phase supports high biomass
786 accumulation, likely from diatoms. Similar results have been reported by Park et al. (2017). They
787 found that the PIP was dFe replete, potentially from biological recycling (Gerringa et al., 2020),
788 compared to an iron-limited ASP. We hypothesise that the connection between glacial meltwater
789 and chl*a* that we found in the ASP is a response to iron input (also observed by Park et al. (2017)
790 during incubation experiments) compared to the PIP, where light and temperature seem to play a

more significant role in driving the phytoplankton bloom variability. Our results suggest potential long-term changes in the phytoplankton community, specifically a shift towards diatoms in the ASE coastal regions during phytoplankton bloom. Hayward et al. (2025) reported a decline in diatoms from 1997 to 2017 in the PIP. However, they observed an increase in diatoms after 2017, linked to regime shift in sea ice. Their study also indicates that diatoms are competitively disadvantaged under iron-depleted conditions. *P. antarctica*, which relies on dFe supplied by ocean circulation, would then tends to dominate in the ASP. Such shifts in phytoplankton composition are likely to affect carbon export, grazing, and higher trophic levels. Additional long-term data on inter-annual variability in phytoplankton composition and physiology will be essential to fully understand these relationships.

Variability in SIC and sea-ice retreat can be influenced by the Amundsen Sea Low (ASL) . We therefore also investigated its potential role on sea-ice variability. We found on average weak spatial negative relationships between SIC and ASL latitude, longitude, mean sector and actual central pressure in both polynyas during the growing seasons (Supplementary Fig. S8), and only slightly significant in the eastern PIP. The weak relationships might be owing to the seasonal variation of the ASL, where its position largely varies during summer, and its impact in shaping coastal sea ice is also greater during winter and autumn in the Amundsen-Bellingshausen region (Hosking et al., 2013). The lack of strong significant relationships overall does not allow us to conclude that the ASL plays an important role in shaping the coastal polynyas landscape and influencing chl*a* variability.

4.3 Limitations and future directions

While it seems reasonable that the higher ASP productivity could be driven by more iron delivered through a stronger meltwater pump downstream of the PIP, our data cannot confirm this hypothesis. To accurately understand the role of iron through the meltwater pump process, we would need to quantify the fraction of meltwater and glacial modified water (mix of CDW and ice shelf meltwater) reaching the ocean surface, together with the iron content. Obtaining this information is challenging over the decadal time scales considered and the method used in our study. Here, our intention was to provide valuable insights into the potential drivers of our

results, and highlight the benefit of remote sensing, in this poorly observed environment. Our work directly aligns with Pan et al. (2025), who investigated the long-term relationship between sea surface glacial meltwater and satellite surface chl*a* in the Western Antarctic Peninsula, and found a strong relationship between the two parameters, highlighting the importance of glacial meltwater discharge in regions prone to extreme and rapid climate changes.

In multimodel climate change simulations, Naughten et al (2018) showed an increase of ice shelves melting up to 90% on average, attributed to more warm CDW on the shelf, due to atmospherically driven changes in local sea-ice formation. More recently, Dinniman et al. (2023) also highlighted the impact of projected atmospheric changes on Antarctic ice sheet melt. They showed that strengthening winds, increasing precipitation and warmer atmospheric temperatures will increase heat advection onto the continental shelf, ultimately increasing basal melt rate by 83% by 2100. Compared to present climate simulations, their simulation showed a 62% increase in total dFe supply to shelf surface waters, while basal melt driven overturning Fe supply increased by 48%. The ice shelf melt and overturning contributions varied spatially, increasing in the Amundsen-Bellingshausen area and decreasing in East Antarctica. This implies that, under future climate change, phytoplankton productivity could show stronger spatial asymmetry around Antarctica. The increasing melting and thinning of ice shelves will eventually result in more numerous calving events and drifting icebergs (Liu et al., 2015). Model simulations stressed the importance of ice shelves and icebergs in delivering dFe to the SO (Death et al., 2014; Person et al., 2019), increasing offshore productivity. As Fe will likely be replenished and sufficient from increasing melting in coastal areas, it is possible that the system will shift from Fe-limited to being limited by nitrate, silicate, or even manganese (Anugerahanti and Tagliabue, 2024), while offshore SO productivity will likely remain Fe-dependent (Oh et al., 2022).

5. Conclusions

Using spatial and multivariate approaches, our study explored the variability of surface chl*a* and NPP in the Amundsen Sea polynyas over the last two decades, with a focus on the main environmental characteristics of the ASE. We found a potential strong relationship between ice shelf melting and surface chl*a* in the ASP, which becomes stronger when year 2001/02 was

removed, a result in agreement with the ASPIRE field studies and previous satellite analyses. On the other hand, we did not find clear evidence of such a relationship in the PIP, where light, sea surface temperature and open water availability seem more important. The differences between the polynyas may lie in hydrographic properties, or the use of satellite remote sensing itself, which cannot tell us about processes such as Fe supply, bioavailability and phytoplankton demand. To gain greater insight, we referred to model simulations that showed the spatial variability in the magnitude of iron sources. Our results call for sustained *in situ* observations (e.g., moorings equipped with trace-metal clean samplers, and physical sensors to better understand year-to-year water mass meltwater fraction and properties) to elucidate these long-term relationships. Satellite observations are a powerful tool to investigate the relationship between glacial meltwater and biological productivity on such time scales, which has until now relied almost exclusively on field observations and modelling. Using such tools, we showed how the relationship between phytoplankton and the environment varies spatially and temporally across 19 years.

Appendices

No appendices are related to the manuscript.

Data availability

Bathymetry data (Amante & Eakins, 2009) was taken from the NOAA website (http://www.ngdc.noaa.gov/mgg/global/global.html). Mixed-layer depth (ECCO Consortium et al., 2021) can be accessed here: https://podaac.jpl.nasa.gov/dataset/ECCO_L4_MIXED_LAYER_DEPTH_05DEG_MONTHLY_V4R4. Satellite surface chlorophyll-*a* and photosynthetically available radiation were downloaded from https://www.globcolour.info/. Sea surface temperature (Huang et al., 2021) can be found here https://psl.noaa.gov/data/gridded/data.noaa.oisst.v2.highres.html. Wind re-analysis data (Hersbach et al., 2020) are available at https://cds.climate.copernicus.eu/datasets/reanalysis-era5-single-levels-monthly-means?tab=download. Sea-ice concentration (Cavalieri et al., 1996) was obtained from https://nsidc.org/data and Net Primary productivity (Behrenfeld and Falkowski, 1997) was downloaded from http://sites.science.oregonstate.edu/ocean.productivity/index.php. Circumpolar

surface model output from Dinniman et al (2020) can be found at https://www.bco-dmo.org/dataset/782848. The Amundsen Sea Low index (Hosking et al., 2016) data are available at http://scotthosking.com/asl_index.

Author contributions

GL conceptualised and led the study; MSD provided the dissolved iron model output. All authors were involved in the interpretation of the results, the revision, and the writing of the final version of the paper.

Competing interest

We declare having no competing interests.

Acknowledgments

We would like to thank the University of Tasmania, the Australian Research Council (ARC) Centre of Excellence for Climate Extremes (CE170100023), and the Australian Centre for Excellence in Antarctic Science (ACEAS; SR200100008) for financial support. Delphine Lannuzel is funded by the ARC through a Future Fellowship (L0026677). Sebastien Moreau received funding from the Research Council of Norway (RCN) for the project "I-CRYME: Impact of CRYosphere Melting on Southern Ocean Ecosystems and biogeochemical cycles" (grant number 335512) and for the Norwegian Centre of Excellence "iC3: Center for ice, Cryosphere, Carbon and Climate" (grand number 332635). Michael Dinniman was supported by the U.S National Science Foundation grant OPP-1643652. We are also grateful to Will Hobbs, Rob Massom and Patricia Yager for their knowledgeable input. We thank Vincent Georges for some preliminary work as part of his masters' internship. We are very grateful to Fernando S. Paolo for his early input and help with the glacial meltwater dataset. We thank the data providers mentioned in the methods section for making their data available and free of charge.

Financial support

All financial support were mentioned in the Acknowledgment section.

References

915 Adusumilli, S., Fricker, H. A., Medley, B., Padman, L., and Siegfried, M. R.: Interannual
916 variations in meltwater input to the Southern Ocean from Antarctic ice shelves, Nat. Geosci., 13,
917 616–620, https://doi.org/10.1038/s41561-020-0616-z, 2020.

918 Alderkamp, A-C., Mills, M. M., van Dijken, G. L., Lann, P., Thuróczy, C-E.,Gerringa, L. J.A.,
919 de Barr, H. J. W., Payne, C. D., Visser, R. J. W., Buma A. G. J., and Arrigo, K. R.: Iron from
920 glaciers fuels phytoplankton blooms in the Amundsen Sea (Southern Ocean): Phytoplankton
921 characteristics and productivity, Deep-Sea Res. II., 71-76, 32-48,
922 https://doi.org/10.1016/j.dsr2.2012.03.005, 2012.
923
924 Amante, C., and Eakins, B.W.: ETOPO1 1 Arc-Minute Global Relief Model: Procedures, Data
925 Sources and Analysis, NOAA Tehnical Memorandum NESDIS NGDC-24. National
926 Geophysical Data Center [data set], NOAA, doi:10.7289/V5C8276M, 2009.
927
928 Anugerahanti, P. and Tagliabue, A.: Response of Southern Ocean Resource Stress in a Changing
929 Climate, Geophys. Res. Lett., 51, e2023GL107870, https://doi.org/10.1029/2023GL107870,
930 2024.

931 Ardyna, M., Claustre, H., Sallée, J-B., D'Ovidio, F., Gentili, B., van Dijken, G. L., D'Ortenzio,
932 F., and Arrigo, K. R.: Delineating environmental control of phytoplankton biomass and
933 phenology in the Southern Ocean, Geophys. Res. Lett., 44, 5016-5024, doi:10.1002/
934 2016GL072428, 2017.

935 Ardyna, M., Mundy, C. J., Mayot, N., Matthes, L. C., Oziel, L., Horvat, C., Leu, E., Assmy, P.,
936 Hill, V., Matrai, P. A., Gale, M., Melnikov, I. A., and Arrigo, K. R.: Under-Ice Phytoplankton
937 Blooms: Shedding Light on the "Invisible" Part of Arctic Primary Production, Front. Mar. Sci.,
938 7, https://doi.org/10.3389/fmars.2020.608032, 2020.

939 Arnscheidt, C. W., Marshall, J., Dutrieux, P., Rye, C. D., and Ramadhan, A.: On the Settling
940 Depth of Meltwater Escaping from beneath Antarctic Ice Shelves, JPO, 51, 2257–2270,
941 https://doi.org/10.1175/JPO-D-20-0286.1, 2021.

942 Arrigo, K. R., Lowry, K. E., and van Dijken, G. L.: Annual changes in sea ice and phytoplankton
943 in polynyas of the Amundsen Sea, Antarctica. Deep-Sea Res. II., 71–76, 5–15.
944 https://doi.org/10.1016/j.dsr2.2012.03.006, 2012.

945 Arrigo, K. R., Robinson, D. H., Worthen, D. L., Dunbar, R. B., DiTullio, G. R., VanWoert, M.,
946 and Lizotte, M. P.: Phytoplankton community structure and the drawdown of nutrients and CO_2
947 in the Southern Ocean, Sci, 283, 5400, 365-367, DOI: 10.1126/science.283.5400.365, 1999.
948
949 Arrigo, K. R. and van Dijken, G. L.: Phytoplankton dynamics within 37 Antarctic coastal
950 polynya systems, J. Geophys. Res. Ocean., 108, https://doi.org/10.1029/2002JC001739, 2003.

951 Arrigo, K. R., van Dijken, G. L., and Strong, A. L.: Environmental controls of marine
952 productivity hot spots around Antarctica, J. Geophys. Res. Ocean., 120, 5545–5565,
953 https://doi.org/10.1002/2015JC010888, 2015.

954 Arrigo, K. R., Worthen, D., Schnell, A., and Lizotte, M. P.: Primary production in Southern
955 Ocean waters, J. Geophys. Res. Ocean., 103, 15587–15600, https://doi.org/10.1029/98JC00930,
956 1998.

957 Assmann, K. M., Jenkins, A., Shoosmith, D. R., Walker, D., Jacobs, S., and and Nicholls, K.:
958 Variability of circumpolar deep water transport onto the Amundsen Sea continental shelf through
959 a shelf break trough. *J. Geophys. Res. Ocean***s**, 118**,** 6603–6620, doi:10.1002/2013JC008871,
960 2013.

961 Behrenfeld, M. J. and Falkowski, P. G.: Photosynthetic rates derived from satellite-based
962 chlorophyll concentration, Limnol. Oceanogr., 42, 1–20,
963 https://doi.org/10.4319/lo.1997.42.1.0001, 1997.

964 Bett, D. T., Holland, P. R., Naveira Garabato, A. C., Jenkins, A., Dutrieux, P., Kimura, S., and
965 Fleming, A.: The Impact of the Amundsen Sea Freshwater Balance on Ocean Melting of the
966 West Antarctic Ice Sheet, J. Geophys. Res. Oceans., 125, https://doi.org/10.1029/2020JC016305,
967 2020.

968 Bhatia, M. P., Kujawinski, E. B., Das, S. B., Breier, C. F., Henderson, P. B., and Charette, M. A.:
969 Greenland meltwater as a significant and potentially bioavailable source of iron to the ocean,
970 Nat. Geosci, 6, 274–278, https://doi.org/10.1038/ngeo1746, 2013.

971 Biddle, L. C., Heywood, K. J., Kaiser, J., and Jenkins, A.: Glacial Meltwater Identification in the
972 Amundsen Sea, JPO, 47, 933–954, https://doi.org/10.1175/JPO-D-16-0221.1, 2017.

973 Boles, E., Provost, C., Garçon, V., Bertosio, C., Athanase, M., Koenig, Z., and Sennéchael, N.:
974 Under-Ice Phytoplankton Blooms in the Central Arctic Ocean: Insights From the First
975 Biogeochemical IAOOS Platform Drift in 2017, J. Geophys. Res. Ocean., 125, e2019JC015608,
976 https://doi.org/10.1029/2019JC015608, 2020.

977 Boyd, P. W., Jickells, T., Law, C. S., Blain, S., Boyle, E. A., Buesseler, K. O., Coale, K. H.,
978 Cullen, J. J., Baar, H. J. W. de, Follows, M., Harvey, M., Lancelot, C., Levasseur, M., Owens, N.
979 P. J., Pollard, R., Rivkin, R. B., Sarmiento, J., Schoemann, V., Smetacek, V., Takeda, S., Tsuda,
980 A., Turner, S., and Watson, A. J.: Mesoscale Iron Enrichment Experiments 1993-2005: Synthesis
981 and Future Directions, Science, 315, 612–617, https://doi.org/10.1126/science.1131669, 2007.

982 Cape, M. R., Vernet, M., Pettit, E. C., Wellner, J., Truffer, M., Akie, G., Domack, E., Leventer,
983 A., Smith, C. R., and Huber, B. A.: Circumpolar Deep Water Impacts Glacial Meltwater Export
984 and Coastal Biogeochemical Cycling Along the West Antarctic Peninsula, Front. Mar. Sci., 6,
985 https://doi.org/10.3389/fmars.2019.00144, 2019.

986 Cavalieri, D., Parkinson, C., Gloersen, P., and Zwally, H. J.: Sea Ice Concentrations from
987 Nimbus-7 SMMR and DMSP SSM/I-SSMIS Passive Microwave Data, Version 1,
988 https://doi.org/10.5067/8GQ8LZQVL0VL, 1996.

Death, R., Wadham, J. L., Monteiro, F., Le Brocq, A. M., Tranter, M., Ridgwell, A., Dutkiewicz, S., and Raiswell, R.: Antarctic ice sheet fertilises the Southern Ocean, BG, 11, 2635–2643, https://doi.org/10.5194/bg-11-2635-2014, 2014.

Dinniman, M. S., St-Laurent, P., Arrigo, K. R., Hofmann, E. E., and Dijken, G. L.: Analysis of Iron Sources in Antarctic Continental Shelf Waters, J. Geophys. Res. Oceans., 125, https://doi.org/10.1029/2019JC015736, 2020.

Dinniman, M. S., St-Laurent, P., Arrigo, K. R., Hofmann, E. E., and van Dijken, G. L.: Sensitivity of the Relationship Between Antarctic Ice Shelves and Iron Supply to Projected Changes in the Atmospheric Forcing, J. Geophys. Res. Ocean., 128, e2022JC019210, https://doi.org/10.1029/2022JC019210, 2023.

Dotto, T. S., Naveira Garabato, A. C., Bacon, S., Holland, P. R., Kimura, S., Firing, Y. L., Tsamados, M., Wåhlin, A. K., and Jenkins, A.: Wind-Driven Processes Controlling Oceanic Heat Delivery to the Amundsen Sea, Antarctica, J. Phys. Oceanogr., 49, 2829–2849, https://doi.org/10.1175/JPO-D-19-0064.1, 2019.

Douglas, C. C., Briggs, N., Brown, P., MacGilchrist, G., and Naveira Garabato, A.: Exploring the relationship between sea ice and phytoplankton growth in the Weddell Gyre using satellite and Argo float data, Ocean Sci., 20, 475–497, https://doi.org/10.5194/os-20-475-2024, 2024.

Dutrieux, P., De Rydt, J., Jenkins, A., Holland, P. R., Ha, H., K., Lee, S. H., Steig, E. J., Ding, Q., Abrahamsen, E. P., and Schröder, M.: Strong sensitivity of Pine Island ice-shelf melting to climate variability, Sci, 343, 6167, 174-178, DOI: 10.1126/science.1244341, 2014.

ECCO Consortium, Fukumori, I., Wang, O., Fenty, I., Forget, G., Heimbach, P., and Ponte, R. M: ECCO Ocean Mixed Layer Depth - Monthly Mean 0.5 Degree 9Version 4 Release 4). ver V4r4. PO.DACC, CA, USA, Dataset accessed [2025-08-22], https://doi.org/10.5067/ECG5M-OML44, 2021.

Forsch, K. O., Hahn-Woernle, L., Sherrell, R. M., Roccanova, V. J., Bu, K., Burdige, D., Vernet, M., and Barbeau, K. A.: Seasonal dispersal of fjord meltwaters as an important source of iron and manganese to coastal Antarctic phytoplankton, Biogeo., 18, 6349–6375, https://doi.org/10.5194/bg-18-6349-2021, 2021.

Golder, MR., and Antoine, D.: Physical drivers of long-term chlorophyll-a variability in the Southern Ocean, Elem. Sci Anth, 13:1, https://doi.org/10.1525/elementa.2024.00077, 2025.

Garabato, A. C. N., Forryan, A., Dutrieux, P., Brannigan, L., Biddle, L. C., Heywood, K. J., Jenkins, A., Firing, Y. L., and Kimura, S.: Vigorous lateral export of the meltwater outflow from beneath an Antarctic ice shelf, Nature, 542, 219–222, https://doi.org/10.1038/nature20825, 2017.

Gerringa, L. J. A., Alderkamp, A.-C., Laan, P., Thuróczy, C.-E., De Baar, H. J. W., Mills, M. M., van Dijken, G. L., Haren, H. van, and Arrigo, K. R.: Iron from melting glaciers fuels the phytoplankton blooms in Amundsen Sea (Southern Ocean): Iron biogeochemistry, Deep-Sea Res. II., 71–76, 16–31, https://doi.org/10.1016/j.dsr2.2012.03.007, 2012.

Gerringa, L. J. A., Alderkamp, A.-C., Laan, P., Thuróczy, C.-E., de Baar, H. J. W., Mills, M. M., van Dijken, G. L., van Haren, H., and Arrigo, K. R.: Corrigendum to "Iron from melting glaciers fuels the phytoplankton blooms in Amundsen Sea (Southern Ocean): iron biogeochemistry" (Gerringa et al., 2012), Deep-Sea Res. II., 177, 104843, https://doi.org/10.1016/j.dsr2.2020.104843, 2020.

Gledhill, M. and Buck, K.: The Organic Complexation of Iron in the Marine Environment: A Review, Front. Microbiol., 3, https://doi.org/10.3389/fmicb.2012.00069. 2012.

Goldberg, D. N., Twelves, A. G., Holland, P. R.. & Wearing, K. G.: The non-local impact of Antarctic subglacial runoff. *Journal of Geophysical Research: Oceans1 128, e2023JC019823.* https://doi.org/10.1029/2023JC01982. 2023.

Ha, H. K., Wåhlin, A. K., Kim, T. W., Lee, S. H., Lee, J. H., Lee, H. J., Hong, C. S., Arneborg, L., Björk, G., and Kalén, O.: Circulation and modification of warm deep water on the central Amundsen shelf, 44, 5, 1493-1501, https://doi.org/10.1175/JPO-D-13-0240.1, 2014.

Hassler, C., Cabanes, D., Blanco-Ameijeiras, S., Sander, S. G., Benner, R., Hassler, C., Cabanes, D., Blanco-Ameijeiras, S., Sander, S. G., and Benner, R.: Importance of refractory ligands and their photodegradation for iron oceanic inventories and cycling, Mar. Fresh. Res., 71, 311–320, https://doi.org/10.1071/MF19213, 2019.

Hawkings, J. R., Wadham, J. L., Tranter, M., Raiswell, R., Benning, L. G., Statham, P. J., Tedstone, A., Nienow, P., Lee, K., and Telling, J.: Ice sheets as a significant source of highly reactive nanoparticulate iron to the oceans, Nat. Commun., 5, 3929, https://doi.org/10.1038/ncomms4929, 2014.

Hayward, A., Wright, S.W., Carroll, D. Law, C. S., Wongpan, P., Gutiérrez-Rodriguez, A., and Pinkerton, M. H.: Antarctic phytoplankton communities restructure under shifting sea-ice regimes. Nat. Clim. Chang. 15, 889–896, https://doi.org/10.1038/s41558-025-02379-x, 2025.

Herraiz-Borreguero, L., Lannuzel, D., van der Merwe, P., Treverrow, A., and Pedro, J. B.: Large flux of iron from the Amery Ice Shelf marine ice to Prydz Bay, East Antarctica, J. Geophys. Res. Ocean., 121, 6009–6020, https://doi.org/10.1002/2016JC011687, 2016.

Hersbach, H., Bell, B., Berrisford, P., Hirahara, S., Horányi, A., Muñoz-Sabater, J., Nicolas, J., Peubey, C., Radu, R., Schepers, D., Simmons, A., Soci, C., Abdalla, S., Abellan, X., Balsamo, G., Bechtold, P., Biavati, G., Bidlot, J., Bonavita, M., De Chiara, G., Dahlgren, P., Dee, D., Diamantakis, M., Dragani, R., Flemming, J., Forbes, R., Fuentes, M., Geer, A., Haimberger, L., Healy, S., Hogan, R. J., Hólm, E., Janisková, M., Keeley, S., Laloyaux, P., Lopez, P., Lupu, C., Radnoti, G., de Rosnay, P., Rozum, I., Vamborg, F., Villaume, S., and Thépaut, J.-N.: The ERA5 global reanalysis, Q. J. R. Meteorol. Soc., 146, 1999–2049, https://doi.org/10.1002/qj.3803, 2020.

Hosking, J. S., Orr, A., Marshall, G. J., Turner, J., and Phillips, T.: The Influence of the Amundsen–Bellingshausen Seas Low on the Climate of West Antarctica and Its Representation

in Coupled Climate Model Simulations, J. Clim., 26, 6633–6648, https://doi.org/10.1175/JCLI-D-12-00813.1, 2013.

Hosking, J. S., Orr, A., Bracegirdle, T. J., and Turner, J.: Future circulation changes off West Antarctica: Sensitivity of the Amundsen Sea Low to projected anthropogenic forcing, Geophys. Res. Lett., 43, 367–376, https://doi.org/10.1002/2015GL067143, 2016.

Huang, B., Liu, C., Banzon, V., Freeman, E., Graham, G., Hankins, B., Smith, T., and Zhang, H.-M.: Improvements of the Daily Optimum Interpolation Sea Surface Temperature (DOISST) Version 2.1, Journal of Climate, 34, 2923-2939. doi: 10.1175/JCLI-D-20-0166.1, 2021.

Jacobs, S. S., Jenkins, A., Giulivi, C. F., and Dutrieux, P.: Stronger ocean circulation and increased melting under Pine Island Glacier ice shelf, Nat. Geo., 4, 519–523, https://doi.org/10.1038/ngeo1188, 2011.

Jena, B. and Pillai, A. N.: Satellite observations of unprecedented phytoplankton blooms in the Maud Rise polynya, Southern Ocean, The Cryosphere, 14, 1385–1398, https://doi.org/10.5194/tc-14-1385-2020, 2020.

Jenkins, A., Dutrieux, P., Jacobs, S. S., McPhail, S. D., Perrett, J. R., Webb, A. T., and White, D.: Observations beneath Pine Island glacier in West Antarctica and implications for its retreat, Nat. Geo., 3, 468-472, https://doi.org/10.1038/NGEO890, 2010.

Jourdain, N. C., Mathiot, P., Merino, N., Durand, G., Le Sommer, J., Spence, P., Dutrieux, P., and Madec, G.: Ocean circulation and sea-ice thinning induced by melting ice shelves in the Amundsen Sea, J. Geophys. Res. Ocean., 122, 2550–2573, https://doi.org/10.1002/2016JC012509, 2017.

Kauko, H. M., Hattermann, T., Ryan-Keogh, T., Singh, A., de Steur, L., Fransson, A., Chierici, M., Falkenhaug, T., Hallfredsson, E. H., Bratbak, G., Tsagaraki, T., Berge, T., Zhou, Q., and Moreau, S.: Phenology and Environmental Control of Phytoplankton Blooms in the Kong Håkon VII Hav in the Southern Ocean, Front. Mar. Sci., 8, https://doi.org/10.3389/fmars.2021.623856, 2021.

Lannuzel, D., Fourquez, M., de Jong, J., Tison, J.-L., Delille, B., and Schoemann, V.: First report on biological iron uptake in the Antarctic sea-ice environment, Polar Biol, 46, 339–355, https://doi.org/10.1007/s00300-023-03127-7, 2023.

Lee, S. H., Kim, B. K., Lim, Y. J., Joo, H., Kang, J. J., Lee, D., Park, J., Ha, S.-Y., and Lee, S. H.: Small phytoplankton contribution to the standing stocks and the total primary production in the Amundsen Sea, BG, 14, 3705–3713, https://doi.org/10.5194/bg-14-3705-2017, 2017.

Lee, Y., Park, J., Jung, J., and Kim, T. W.: Unpredecedented differences in phytoplnakton community structures in the Amundsen Sea polynyas, West Antarctica, Envrion. Res. Lett. 17, 114022, 10.1088/1748-9326/ac9a5f, 2022.

van Leeuwe, M. A., Webb, A. L., Venables, H. J., Visser, R. J. W., Meredith, M., P., Elzenga J. T. M., and Stefels, J.: Annual patterns in phytoplnakton phenology in Antarctic coastal waters explained by environmental drivers, Limnol. Oceanogr., 65, 1651-1668, https://doi.org/10.1002/lno.11477, 2020.

Liniger, G., Strutton, P. G., Lannuzel, D., and Moreau, S.: Calving event led to changes in phytoplankton bloom phenology in the Mertz polynya, Antarctica, J. Geophys. Res. Oceans., 125, e2020JC016387, https://doi.org/10.1029/2020JC016387, 2020.

Liu, Y., Moore, J. C., Cheng, X., Gladstone, R. M., Bassis, J. N., Liu, H., Wen, J., and Hui, F.: Ocean-driven thinning enhances iceberg calving and retreat of Antarctic ice shelves, Proc. Nat. Acad. Sci., 112, 3263–3268, https://doi.org/10.1073/pnas.1415137112, 2015.

van Manen, M., Aoki, S., Brussaard, C. P. D., Conway, T. M., Eich, C., Gerringa, L., Jung, J., Kim, T.-W., Lee, S. H., Lee, Y., Reichart, G.-J., Tian, H., Wille, F., and Middag, R.: The role of the Dotson Ice Shelf and circumpolar deep water as driver and source of dissolved and particulate iron and manganese in the Amundsen Sea polynya, Southern Ocean, Mar. Chem., 104161, https://doi.org/10.1016/j.marchem.2022.104161, 2022.

Marchese, C., Albouy, C., Tremblay, J.-É., Dumont, D., D'Ortenzio, F., Vissault, S., and Bélanger, S.: Changes in phytoplankton bloom phenology over the North Water (NOW) polynya: a response to changing environmental conditions, Polar Biol, 40, 1721–1737, https://doi.org/10.1007/s00300-017-2095-2, 2017.

Maritorena, S., and Siegel, D. A.: Consistent merging of satellite ocean color data sets using a bio-optical model, Rem. Sens. Eviron., 94, 429-440, https://doi.org/10.1016/j.rse.2004.08.014, 2005.

McClish, S., and Bushinsky, S. M.: Majority of Southern Ocean seasonal ice zone bloom net community production precedes total ice retreat, Geophys. Res. Lett., 50, e2023GL103459. https://doi.org/10.1029/2023GL103459, 2023.

Meredith, M., Sommerkorn, M., Cassotta, S., Derksen, C., Ekaykin, A., Hollowed, A., Kofinas, G., Mackintosh, A., Melbourne-Thomas, J., Muelbert, M.M.C., Ottersen, G., Pritchard, H., and Schurr, E.A.G.: Polar Regions. In: *IPCC Special Report on the Ocean and Cryosphere in a Changing Climate* [H.-O. Pörtner, D.C. Roberts, V. Masson-Delmotte, P. Zhai, M. Tignor, E. Poloczanska, K. Mintenbeck, A. Alegría, M. Nicolai, A. Okem, J. Petzold, B. Rama, N.M. Weyer (eds.)]. Cambridge University Press, Cambridge, UK and New York, NY, USA, pp. 203-320, https://doi.org/10.1017/9781009157964.005, 2019.

Mills, M. M., Lindsey, R.K., van Dijken, G. L., Alderkamp, C-A., Berg, G. M., Robinson, D. H., Welschmeyer, N. A and Arrigo, K. R.: Photophysiology in two Southern Ocean phytoplankton taxa: photosynthesis of phaeocystis antarctica (prymnesiophyceae) and fragiloriapsis cyclindrus (bacillariophyceae) under simulated mixed-layer irradiance, J. Phycol, 46, 1114-1127, https://doi.org/10.1111/j.1529-8817.2010.00923.x, 2010.

Mills, M. M., Alderkamp, C-A., Thuróczy, C-E., van Dijken, G. L., Laan, P., de Barr, H. J. W. and Arrigo, K. R.: Phytoplankton biomass and pigment responses to Fe amendments on the Pine Island and Amundsen polynyas, Deep-Sea Res. II., 71-76, 61-76, https://doi.org/10.1016/j.dsr2.2012.03.008, 2012.

Morales Maqueda, M. A.: Polynya Dynamics: a Review of Observations and Modeling, Rev. Geophys., 42, RG1004, https://doi.org/10.1029/2002RG000116, 2004.

Moreau, S., Mostajir, B., Bélanger, S., Schloss, I. R., Vancoppenolle, M., Demers, S., and Ferreyra, G. A.: Climate change enhances primary production in the western Antarctic Peninsula, Global Change Biology, 21, 2191–2205, https://doi.org/10.1111/gcb.12878, 2015.

Naughten, K. A., Holland, P. R., and De Rydt, J.: Unavoidable future increase in West Antarctic ice-shlef melting over the twenty-fist century, Nat. Clim. Change., 13, 1222-1228, https://doi.org/10.1038/s41558-023-01818-x, 2023.

Naughten, K. A., Meissner, K. J., Galton-Fenzi, B. K., England, M. H., Timmermann, R., and Hellmer, H. H.: Future Projections of Antarctic Ice Shelf Melting Based on CMIP5 Scenarios, J. Clim., 31, 5243–5261, https://doi.org/10.1175/JCLI-D-17-0854.1, 2018.

Nunes, G.S., Ferreira, A. and Brito, A.C. Long-term satellite data reveals complex phytoplankton dynamics in the Ross Sea, Antarctica. Commun. Earth. Environ., 6, 864, https://doi.org/10.1038/s43247-025-02590-w, 2025.

Oh, J.-H., Noh, K. M., Lim, H.-G., Jin, E. K., Jun, S.-Y., and Kug, J.-S.: Antarctic meltwater-induced dynamical changes in phytoplankton in the Southern Ocean, Environ. Res. Lett., 17, 024022, https://doi.org/10.1088/1748-9326/ac444e, 2022.

Oliver, H., St-Laurent, P., Sherrell, R. M., and Yager, P. L.: Modeling Iron and Light Controls on the Summer *Phaeocystis antarctica* Bloom in the Amundsen Sea Polynya, Global Biogeochem. Cycles, 2018GB006168, https://doi.org/10.1029/2018GB006168, 2019.

Pan, J. B., Gierach, M. M., Stammerjohn, S., Schofiled, O., Meredith, M. P., Reynolds, R. A., vernet, M., Haumann, F. A., Orona, A. J., and Miller, C. E.: Impact of glacial meltwater on phytoplankton biomass along the Western Antarctic Peninsula. Comm. Earth. Environ., 6(456). https://doi.org/10.1038/s43247-025-02435-6. 2025

Paolo, F. S., Fricker, H. A., and Padman, L.: Volume loss from Antarctic ice shelves is accelerating, Science, 348, 327–331, https://doi.org/10.1126/science.aaa0940, 2015.

Paolo, F. S., Fricker, H. A., and Padman, L.: Constructing improved decadal records of Antarctic ice shelf height change from multiple satellite radar altimeters, Remote Sens. Environ. 177, 192–205, https://doi.org/10.1016/j.rse.2016.01.026, 2016.

Paolo, F. S., Gardner, A. S., Greene, C. A., Nilsson, J., Schodlok, M. P., Schlegel, N.-J., and Fricker, H. A.: Widespread slowdown in thinning rates of West Antarctic ice shelves, TC, 17, 3409–3433, https://doi.org/10.5194/tc-17-3409-2023, 2023.

Park, J., Kuzminov, F. I., Bailleul, B., Yang, E. J., Lee, S., Falkowski, P. G., and Gorbunov, M. Y.: Light availability rather than Fe controls the magnitude of massive phytoplankton bloom in the Amundsen Sea polynyas, Antarctica: Light availability rather than Fe controls phytoplankton bloom, Limnol. Oceanogr., 62, 2260–2276, https://doi.org/10.1002/lno.10565, 2017.

Park, J., Kim, J.-H., Kim, H., Hwang, J., Jo, Y.-H., and Lee, S. H.: Environmental Forcings on the Remotely Sensed Phytoplankton Bloom Phenology in the Central Ross Sea Polynya, J. Geophys. Res. Ocean., 124, 5400–5417, https://doi.org/10.1029/2019JC015222, 2019.

Person, R., Aumont, O., Madec, G., Vancoppenolle, M., Bopp, L., and Merino, N.: Sensitivity of ocean biogeochemistry to the iron supply from the Antarctic Ice Sheet explored with a biogeochemical model, BG, 16, 3583–3603, https://doi.org/10.5194/bg-16-3583-2019, 2019.

Pritchard, H. D., Ligtenberg, S. R. M., Fricker, H. A., Vaughan, D. G., van den Broeke, M. R., and Padman, L.: Antarctic ice-sheet loss driven by basal melting of ice shelves, Nat., 484, 502–505, https://doi.org/10.1038/nature10968, 2012.

Racault, M.-F., Le Quéré, C., Buitenhuis, E., Sathyendranath, S., and Platt, T.: Phytoplankton phenology in the global ocean, Ecol. Indic., 14, 152–163, https://doi.org/10.1016/j.ecolind.2011.07.010, 2012.

Randall-Goodwin, E., Meredith, M. P., Jenkins, A., Yager, P. L., Sherrell, R. M., Abrahamsen, E. P., Guerrero, R., Yuan, X., Mortlock, R. A., Gavahan, K., Alderkamp, A.-C., Ducklow, H., Robertson, R., and Stammerjohn, S. E.: Freshwater distributions and water mass structure in the Amundsen Sea Polynya region, Antarctica, Elem. Sci. Anth., 3, 000065, https://doi.org/10.12952/journal.elementa.000065, 2015.

Rignot, E., Jacobs, S., Mouginot, J., and Scheuchl, B.: Ice-Shelf Melting Around Antarctica, Sci, 341, 266–270, https://doi.org/10.1126/science.1235798, 2013.

Rignot, E., Mouginot, J., Scheuchl, B., van den Broeke, M., van Wessem, M. J., and Morlighem, M.: Four decades of Antarctic Ice Sheet mass balance from 1979–2017, Proc. Nat. Acad .Sci., 116, 4, 1095–1103, https://doi.org/10.1073/pnas.1812883116, 2019.

Ryan-Keogh, T. J., Thomalla, S. J., Chang, N., and Moalusi, T.: A new global oceanic multi-model net primary productivity data product, Earth Syst. Sci. Data, 15, 4829–4848, https://doi.org/10.5194/essd-15-4829-2023, 2023.

Sari El Dine, Z., Guinet, C., Picard, B., Thyssen, M., Duforêt-gaurier, L., and El Hourany, R.:Influence of the phytoplankton community structure on the southern elephant seals' foraging activity within the Southern Ocean, Commun. Biol., 8, 620, https://doi.org/10.1038/s42003-025-08049-0, 2025.

Scambos, T., Bell, R. E., Alley, R. B., Anandakrishnan, S., Bromwich, D. H., Brunt, K., Christianson, K., Creyts, T., Das, S. B., DeConto, R., Dutrieux, P., Fricker, H. A., Holland, D., MacGregor, J., Medley, B., Nicolas, J. P., Pollard, D., Siegfried, M. R., Smith, A. M., Steig, E. J., Trusel, L. D., Vaughan, D. G., and Yager, P. L.: How much, how fast?: A science review and

outlook for research on the instability of Antarctica's Thwaites Glacier in the 21st century, Glob. Planet. Change.,153, 16-34, https://doi.org/10.1016/j.gloplacha.2017.04.008, 2017.

Silsbe, G. M., Behrenfeld, M. J., Halsey, K. H., Milligan, A. J., and Westberry, T. K.: The CAFE model: A net production model for global ocean phytoplankton, Global Biogeochem. Cycles., 30, 1756–1777, doi:10.1002/2016GB005521, 2016.

Shepherd, A., Ivins, E., Rignot, E., Smith, B., van den Broeke, M., Velicogna, I., Whitehouse, P., Briggs, K., Joughin, I., Krinner, G., Nowicki, S., Payne, T., Scambos, T., Schlegel, N., A, G., Agosta, C., Ahlstrøm, A., Babonis, G., Barletta, V., Blazquez, A., Bonin, J., Csatho, B., Cullather, R., Felikson, D., Fettweis, X., Forsberg, R., Gallee, H., Gardner, A., Gilbert, L., Groh, A., Gunter, B., Hanna, E., Harig, C., Helm, V., Horvath, A., Horwath, M., Khan, S., Kjeldsen, K. K., Konrad, H., Langen, P., Lecavalier, B., Loomis, B., Luthcke, S., McMillan, M., Melini, D., Mernild, S., Mohajerani, Y., Moore, P., Mouginot, J., Moyano, G., Muir, A., Nagler, T., Nield, G., Nilsson, J., Noel, B., Otosaka, I., Pattle, M. E., Peltier, W. R., Pie, N., Rietbroek, R., Rott, H., Sandberg-Sørensen, L., Sasgen, I., Save, H., Scheuchl, B., Schrama, E., Schröder, L., Seo, K.-W., Simonsen, S., Slater, T., Spada, G., Sutterley, T., Talpe, M., Tarasov, L., van de Berg, W. J., van der Wal, W., van Wessem, M., Vishwakarma, B. D., Wiese, D., Wouters, B., and The IMBIE team: Mass balance of the Antarctic Ice Sheet from 1992 to 2017, Nat., 558, 219–222, https://doi.org/10.1038/s41586-018-0179-y, 2018.

Sherrell, R. M., Lagerström, M. E., Forsch, K. O., Stammerjohn, S. E., and Yager, P. L.: Dynamics of dissolved iron and other bioactive trace metals (Mn, Ni, Cu, Zn) in the Amundsen Sea Polynya, Antarctica, Elementa: Sci. Anthrop., 3, 000071, https://doi.org/10.12952/journal.elementa.000071, 2015.

Siegel, D. A., Doney, S. C., and Yoder, J. A.: The North Atlantic Spring Phytoplankton Bloom and Sverdrup's Critical Depth Hypothesis, Science, 296, 730–733, https://doi.org/10.1126/science.1069174, 2002.

Smith, A. J. R., Nelson, T., Ratnarajah, L., Genovese, C., Westwood, K., Holmes, T. M., Corkill, M., Townsend, A. T., Bell, E., Wuttig, K., and Lannuzel, D.: Identifying potential sources of iron-binding ligands in coastal Antarctic environments and the wider Southern Ocean, Front. Mar. Sci., 9, https://doi.org/10.3389/fmars.2022.948772, 2022.

Soppa, M. A., Völker, C., and Bracher, A.: Diatom Phenology in the Southern Ocean: Mean Patterns, Trends and the Role of Climate Oscillations, Remote Sens., 8, 420, https://doi.org/10.3390/rs8050420, 2016.

Stammerjohn, S. E., Martinson, D. G., Smith, R. C., and Iannuzzi, R. A.: Sea ice in the western Antarctic Peninsula region: Spatio-temporal variability from ecological and climate change perspectives, Deep-Sea Res. II., 55, 2041–2058, https://doi.org/10.1016/j.dsr2.2008.04.026, 2008.

Stoer, A. C., and Fennel, K.: Carbon-centric dynamics of Earth's marine phytoplankton, Proc. Nat. Acad. Sci., 121, 45, e2405354121, https://doi.org/10.1073/pnas.2405354121 , 2024.

St-Laurent, P., Yager, P. L., Sherrell, R. M., Stammerjohn, S. E., and Dinniman, M. S.: Pathways and supply of dissolved iron in the Amundsen Sea (Antarctica), J. Geophys. Res. Oceans., 122, 7135–7162, https://doi.org/10.1002/2017JC013162, 2017.

St-Laurent, P., Yager, P. L., Sherrell, R. M., Oliver, H., Dinniman, M. S., and Stammerjohn, S. E.: Modeling the Seasonal Cycle of Iron and Carbon Fluxes in the Amundsen Sea Polynya, Antarctica, J. Geophys. Res. Oceans., 124, 1544–1565, https://doi.org/10.1029/2018JC014773, 2019.

Tagliabue, A., Bowie, A. R., DeVries, T., Ellwood, M. J., Landing, W. M., Milne, A., Ohnemus, D. C., Twining, B. S., and Boyd, P. W.: The interplay between regeneration and scavenging fluxes drives ocean iron cycling, Nat Commun, 10, 4960, https://doi.org/10.1038/s41467-019-12775-5, 2019.

Tamsitt, V., England, M. H., Rintoul, S. R., and Morrison, A. K.: Residence Time and Transformation of Warm Circumpolar Deep Water on the Antarctic Continental Shelf, Geophys. Res. Lett., 48, e2021GL096092, https://doi.org/10.1029/2021GL096092, 2021.

Tamura, T. P., Nomura, D., Hirano, D., Tamura, T., Kiuchi, M., Hashida, G., Makabe, R., Ono, K., Ushio, S., Yamazaki, K., Nakayama, Y., Takahashi, K. D., Sasaki, H., Murase, H., and Aoki, S.: Impacts of basal melting of the Totten Ice Shelf and biological productivity on marine biogeochemical components in Sabrina Coast, East Antarctica, Global Biogeochem. Cycles., 37, e2022GB007510, https://doi.org/10.1029/2022GB007510, 2023.

Thomalla, S.J., Nicholson, SA., Ryan-Keogh, T.J. *et al.* Widespread changes in Southern Ocean phytoplankton blooms linked to climate drivers. Nat. Clim. Chang. 13, 975–984, https://doi.org/10.1038/s41558-023-01768-4, 2023.

Thuróczy, C.-E., Alderkamp, A.-C., Laan, P., Gerringa, L. J. A., Mills, M. M., van Dijken, G. L., De Baar, H. J. W., and Arrigo, K. R.: Key role of organic complexation of iron in sustaining phytoplankton blooms in the Pine Island and Amundsen Polynyas (Southern Ocean), Deep-Sea Res. II., 71–76, 49–60, https://doi.org/10.1016/j.dsr2.2012.03.009, 2012.

Turner, J., Hosking, J. S., Marshall, G. J., Phillips, T., and Bracegirdle, T. J.: Antarctic sea ice increase consistent with intrinsic variability of the Amundsen Sea Low, Clim. Dyn., 46, 2391–2402, https://doi.org/10.1007/s00382-015-2708-9, 2016.

Vaillancourt, R. D., Sambrotto, R. N., Green, S., and Matsuda, A.: Phytoplankton biomass and photosynthetic competency in the summertime Mertz Glacier Region of East Antarctica, Deep-Sea Res. II., 50, 1415–1440, https://doi.org/10.1016/S0967-0645(03)00077-8, 2003.

Westberry, T., Behrenfeld, M. J., Siegel, D. A., and Boss, E.: Carbon-based primary productivity modeling with vertically resolved photoacclimation, Global Biogeoch. Cycle., 22, GB2024, doi:10.1029/2007GB003078, 2008.

Yager, P. L., Sherrell, R. M, Stammerjohn, S., Alderkamp, A.-C., Schofield, O., Abrahamsen, P., Arrigo, K., Bertilsson, S., Garay, L., Guerrero, R., Lowry, K., Moksnes, P.-O., Ndungo, K., Post,

A., Randall-Goodwin, E., Riemann, L., Severmann, S., Thatje, S., van Dijken, G., and Wilson, S.: ASPIRE: The Amundsen Sea Polynya International Research Expedition, Oceanog., 25, 40–53, https://doi.org/10.5670/oceanog.2012.73, 2012.

Yager P. L, Sherrell, R.M., Stammerjohn, S.E., Ducklow, H. W., Schofiled, O., Ingall E.D., Wilson, S. E., Lowry, K. E., Willismd, C. M., Riemman, L., Bertilsson, S., Alderkamp, A-C., Dinasquet, J., Logares, R., Richert, I., Sipler, R. E., Melara A. J., Mu, L., Newstead, R. G., Post, A. F., Swalethorp, R and van Dijken, G. L.: A carbon budget for the Amundsen Sea Polynya, Antarctica: Estimating net community production and export in a highly productive polar ecosystem, Elem. Sci. Anth., 4, 000140, doi: 10.12952/journal.elementa.000140, 2016.

Yu, L.-S., He, H., Leng, H., Liu, H., and Lin, P.: Interannual variation of summer sea surface temperature in the Amundsen Sea, Antarctica, Front. Mar. Sci., 10, https://doi.org/10.3389/fmars.2023.1050955, 2023.

Zheng, Y., Heywood, K. J., Webber, B. G. M., Stevens, D. P., Biddle, L. C., Boehme, L., and Loose, B.: Winter seal-based observations reveal glacial meltwater surfacing in the southeastern Amundsen Sea, Commun. Earth. Environ., 2, 1–9, https://doi.org/10.1038/s43247-021-00111-z, 2021.